

# RSC Advances



This is an *Accepted Manuscript*, which has been through the Royal Society of Chemistry peer review process and has been accepted for publication.

*Accepted Manuscripts* are published online shortly after acceptance, before technical editing, formatting and proof reading. Using this free service, authors can make their results available to the community, in citable form, before we publish the edited article. This *Accepted Manuscript* will be replaced by the edited, formatted and paginated article as soon as this is available.

You can find more information about *Accepted Manuscripts* in the [Information for Authors](#).

Please note that technical editing may introduce minor changes to the text and/or graphics, which may alter content. The journal's standard [Terms & Conditions](#) and the [Ethical guidelines](#) still apply. In no event shall the Royal Society of Chemistry be held responsible for any errors or omissions in this *Accepted Manuscript* or any consequences arising from the use of any information it contains.

Cite this: DOI: 10.1039/c0xx00000x

www.rsc.org/xxxxxx

Paper

## Magneto-structural correlation, antioxidant, DNA interaction and growth inhibition activities of new chloro-bridged phenolate complexes

Perumal Gurumoorthy,<sup>a</sup> Dharmasivam Mahendiran,<sup>a</sup> Durai Prabhu,<sup>b</sup> Chinnasamy Arulvasu<sup>b</sup> and Aziz Kalilur Rahiman,<sup>\*a</sup>

Received (in XXX, XXX) Xth XXXXXXXXX 20XX, Accepted Xth XXXXXXXXX 20XX  
DOI: 10.1039/b000000x

A new class of chloro-bridged dinuclear nickel(II) and copper(II) phenolate complexes (**1–8**) were synthesized from 4-substituted-2-((2-(piperazin-1-yl)ethylimino)methyl)phenols (L<sup>1–4</sup>) and characterized. The XRD analysis of complexes **4** and **8** consist of two mononuclear units connected through a bridged chlorine atom that gives dinuclear complexes. The stability of complexes has been determined using a spectrophotometric method. Complexes **5–8** possess significant antioxidant activity against DPPH radical. The binding studies of complexes with CT-DNA suggest partial intercalative/electrostatic interaction and the cleavage ability on pBR322 DNA shows the involvement of the hydroxyl radical as an intermediate in the cleavage reaction. The IC<sub>50</sub> value of complexes **2**, **6** and **8** against HepG2 cell line is comparable with that of cisplatin. To find the extent of nuclear chromatin cleavage, propidium iodide staining and comet assays were employed. Among the newly synthesized complexes, copper(II) complexes exhibited superior biological activity when compared to its nickel(II) analogues.

### Introduction

DNA is storage and carrier of genetic information in a cell and it is the primary intracellular target of anticancer drugs. The interaction between the small molecules and DNA can cause DNA damage, blocking the division of cancer cells, and resulting in cell death.<sup>1</sup> The DNA cleavage is an enzymatic reaction which comprises various biological processes as well as biotechnological manipulation of genetic material. Nowadays, exploring and designing novel molecules capable of interacting with DNA, and triggering apoptosis is one of the strategies for researchers to discover effective DNA-targeted anticancer drugs for chemotherapy.<sup>2</sup>

In modern medicinal field, widely and effectively used antitumor drugs are Pt-based cisplatin [*cis*-diamminedichloro platinum(II)], carboplatin [*cis*-diammine(cyclobutane-1,1-di carboxylato-O,O')platinum(II)], and oxaliplatin [((1*R*,2*R*)-cyclo hexane-1,2-diamine)(ethanedioato-O,O')platinum(II)], but they possess inherent limitations such as ototoxicity, nephrotoxicity, peripheral neuropathy and neurotoxicity, nausea, myelotoxicity, and tumor resistance.<sup>3</sup> Hence, the efforts to mitigate the

drawbacks have prompted researchers to develop other transition metal-based drugs. In this connection, attempts are being made to replace these drugs with more efficacious, less toxic, and target specific non-covalently DNA binding (Intercalation, groove binding and external static electronic effects) chemotherapeutic agents. Among the DNA binding modes, intercalation is the most important one, in which the molecules can intercalate between the base-pairs of double helix DNA, forming  $\pi$ - $\pi$  overlapping interaction, and it is related to the antitumor activity of the molecule.<sup>4</sup> Nickel<sup>5</sup> and copper<sup>6</sup> complexes are regarded as most promising alternatives to platinum complexes as anticancer drugs. Nickel(II) complexes display interesting binding and cleavage reactivity with the nucleic acids.<sup>7</sup> Copper is known to play significant role in biological systems, as pharmacological agents and copper(II) complexes are found to exhibit prominent antitumor activity.<sup>8</sup>

Phenolic Schiff base ligands have received increasing attention because of their ease of formation, mixed hard-soft donor character, versatile coordination behavior and their diversified applications.<sup>9</sup> Transition metal ions play a pivotal role in a vast number of diverse biological processes, and their metal complexes have been widely exploited, because of their unique spectral, electrochemical, magnetic and catalytic signatures but also due to the fact that by changing the ligand environment one can tune the DNA interaction of a metal complex.<sup>10</sup> A further reason for using metal containing compounds as structural scaffolds relates to the kinetic stabilities of their coordination spheres in the biological environment.<sup>11</sup> In past decades, several phenolic based transition metal complexes were reported as they are avid DNA intercalative binders as well as DNA cleavers.<sup>12</sup>

<sup>a</sup> Post-Graduate and Research Department of Chemistry, The New College (Autonomous), Chennai-600 014, Tamil Nadu, India  
Fax: +91 44 2835 2883

E-mail: akrahmanjkr@gmail.com

<sup>b</sup> Department of Zoology, University of Madras, Guindy Maraimalai Campus, Chennai-600 025, Tamil Nadu, India

† Electronic supplementary information (ESI) available: Tables S1–S5, Scheme S1 and Fig. S1–S10, See DOI: 10.1039/b000000x/

Moreover, transition metal complexes are intensely coloured due to localized MLCT (metal to ligand charge transfer transition), and this transition is particularly important as it is perturbed when complex interacts with DNA, providing a spectroscopic probe.

The foregoing facts stimulated us to focus on the studies of biological activities of new halo-bridged dinuclear complexes containing phenolate ligands, which is continuation of our recent report<sup>13</sup>. Amongst the metal ions chosen, we have opted for bio-compatible metal ions, Ni and Cu. These metal complexes are better suited for medical applications because of their favorable rate of ligand exchange and their ability to mimic iron binding to certain bio-molecules. Herein, we report the synthesis and characterization of chloro-bridged dinuclear nickel(II) and copper(II) complexes containing Schiff base ligand, 4-substituted -2-((2-(piperazin-1-yl)ethylimino)methyl)phenol. Antioxidant DNA interaction and growth inhibitory activities of complexes were performed in order to investigate their biological efficacy.

## Results and Discussion

### Synthesis and spectral properties

The chloro-bridged dinuclear nickel(II) and copper(II) complexes (1–8) have been isolated by direct reaction of ligands (L<sup>1–4</sup>) with an equimolar ratio of metal(II) chlorides in methanol. The ligands were used without further purification for the complexation reactions. All complexes are obtained in good yield and, they are soluble in H<sub>2</sub>O, DMF, DMSO and 5 mM Tris-HCl/50 mM NaCl buffer (pH 7.2). The synthesized metal complexes were characterized by means of the spectroscopic methods. All the resulted complexes are characterized by the molar ratio between the ligand and metal ion (2:2). The following series of complexes have been obtained and crystallographically characterized.

IR spectra of complexes are compared with those of free ligands to gain evidence for the coordination mode with the metal ions. All complexes exhibit bands in the region of 1655–1637 and 1309–1290 cm<sup>-1</sup> due to  $\nu(\text{C}=\text{N})$  and  $\nu(\text{Ar}-\text{O})$ , respectively, which were observed at lower frequency than that of free ligands, suggest the coordination *via* imine nitrogen and phenoxide atom, and further confirmed by single crystal XRD structure of complexes 4 and 8. A broad band in the region 3452–3379 cm<sup>-1</sup> indicates  $\nu(\text{O}-\text{H})$  stretching of methanol/water and water molecules for nickel(II) and copper(II) complexes, respectively, and the broadness of O–H stretching is due to hydrogen bonding. All complexes exhibit a medium intensity bands in the region of 2964–2929 and 1549–1524 cm<sup>-1</sup> due to N–H stretching and bending of piperazinium ion,<sup>14</sup> respectively. The ESI-MS results of complexes 1–8 exhibit peaks corresponds to the half unit of the complexes.

The <sup>1</sup>H NMR spectra (Fig. S1) of diamagnetic nickel(II) complexes (1–4) show the considerable changes in the chemical shift of the proton signals when compared with the respective ligands, which we have reported recently.<sup>13</sup> The complexes exhibit the signal for the coordinated azomethine proton at 8.42–8.54 ppm, and these are shifted downfield with respect to the corresponding resonance in the free ligands, indicating that the metal-nitrogen bond is retained in solution. The signals of aromatic (6.74–7.64 ppm) and aliphatic protons (methyl and methylene protons; 2.01–3.72 ppm) appear in their usual positions with slight downfield shifts when compared with the

free ligands. The resonance signal of the NH proton is appeared to be shifted significantly. Further, the broad signal (10.94–10.99 ppm) was observed for the OH proton of the methanol. The NMR spectra gave additional information about the structure of the complexes, which are consistent with the crystal structure of complex 4.

In DMF medium, complexes 1–8 exhibit two intense bands in the UV region (250–400 nm) attributed to the intraligand charge transfer transitions ( $\pi-\pi^*$ ,  $n-\pi^*$ ). The bathochromic shift of  $n-\pi^*$  transition band in complexes suggests the coordination of azomethine with metal center.<sup>15</sup> In the visible region, the nickel(II) complexes (1–4) shows two absorption bands around 624–644 and 930–973 nm whereas the copper(II) complexes (5–8) exhibit one absorption band in the region of 655–668 nm characteristic of metal(II) ion located in distorted octahedral<sup>16</sup> and square-pyramidal<sup>17</sup> environment, respectively. The crystal structure of complexes 4 and 8 have been determined by using single crystal XRD analysis which is consistent with the absorption spectral data and hence the proposed structure of complexes.

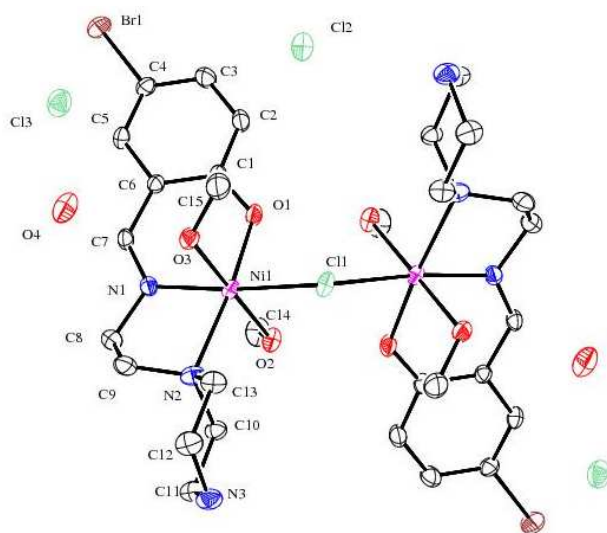


**Fig. 1** ORTEP representation of complex 4 showing an atom numbering scheme and displacement ellipsoid (30% probability level). All the hydrogen atoms are omitted for clarity.

### Description of crystal structure of [(NiL<sup>4</sup>(CH<sub>3</sub>OH)<sub>2</sub>)( $\mu$ -Cl)](Cl)<sub>3</sub>·(H<sub>2</sub>O)<sub>2</sub>, 4

Suitable single crystals of green coloured nickel(II) complex [(NiL<sup>4</sup>(CH<sub>3</sub>OH)<sub>2</sub>)( $\mu$ -Cl)](Cl)<sub>3</sub>·(H<sub>2</sub>O)<sub>2</sub>, 4 was obtained by slow evaporation of the reaction mixture for several days in dark room which crystallizes in a monoclinic space group C2/c. Half of the title molecule forms the asymmetric unit and two halves of the molecule are related through centre of inversion. The ORTEP diagram of the molecule 4 showing the atom numbering scheme is given in Fig. 1, while their selected bond lengths and angles are

given in **Table S1**. The measured unit cell dimensions are  $a = 10.1699(4)$ ,  $b = 16.8523(8)$ ,  $c = 24.8924(11)$  Å,  $\beta = 98.768(2)$  and  $Z = 4$ . The solved structure contains one mononuclear Ni(II) unit with an half coordinating chlorine atom which bridges the another half unit through a 2-fold axis along  $[0\ 1\ 0]$  direction at  $(1/2, y, 3/4)$  to form the title compound. Apart from these, the structure contains three non coordinating chloride anions and two water molecules. The symmetry operation connecting the bridging chlorine atom is about  $1 - x, y, 3/2 - z$ .

The nickel(II) ion in complex is hexacoordinated and best described as a distorted octahedral coordination geometry with two nitrogen atom, an imine (N1) and piperazine (N2), one phenolate (O1) and two methanol solvent (O2, O3) oxygen atoms in addition to one bridged chlorine (Cl1) atom between the metal centers Ni(1) and Ni(2). The bond distances of Ni(1)–N(1), Ni(1)–N(2), Ni(1)–O(1) and Ni(1)–Cl(1) are 2.0085(18), 2.222(2), 1.9974(16) and 2.388(5), respectively. The fifth and sixth coordination positions of the nickel(II) ion is occupied by two methanol solvent molecules with Ni(1)–O(2) and Ni(1)–O(3) distance of 2.0748(17) and 2.1181(16) Å, respectively and O(2)–Ni(1)–O(3) angle of 176.51(7)°. The deprotonation of phenolic hydrogen atom followed by the coordination of nickel with oxygen atom leads to shortening of carbon-oxygen bond and lengthening of carbon-carbon bond. For example the observed C(1)–O(1) bond length is 1.302(3) Å as against 1.351(3) Å for free bromophenol related Schiff base ligand and C(1)–C(2) and C(1)–C(6) bond lengths are 1.401(4) and 1.422(3) Å, respectively, which are higher than the aromatic C–C distances of the same bromophenol related Schiff base ligand.<sup>18</sup> The dimeric complex  $[\text{NiL}^4(\text{CH}_3\text{OH})_2(\mu\text{-Cl})](\text{Cl})_3(\text{H}_2\text{O})_2$  associates with a

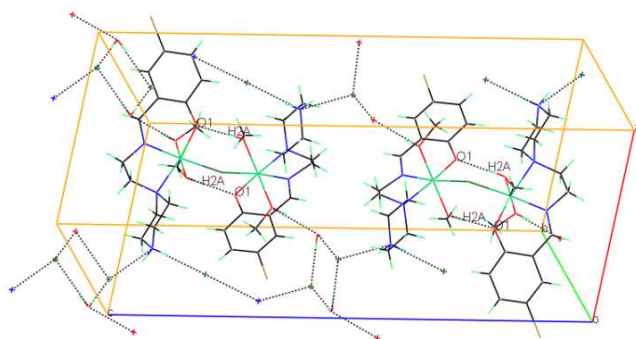


**Fig. 2** Intra- and intermolecular hydrogen bonding network in complex 4.

Ni(1)–Ni(1)#1 distance of 4.096(4) Å, which is shorter than that of reported dinuclear chloro-bridged Ni(II) complex.<sup>19</sup>

Non-covalent (like  $\pi$ -stacking) interactions with aryl hydrogen and hydrogen bonding network are important class in supramolecular chemistry and crystal engineering.<sup>20</sup> The molecular packing in the crystalline solid is constituted by intramolecular and intermolecular hydrogen and halogen bonds (**Fig. 2**) and the hydrogen bonding parameters are listed in **Table S2**. The lattice chloride anions are able to act as a proton acceptor, interacting with the partially charged N–H group and O–H group of lattice water molecules. The intramolecular

hydrogen bonding exhibit between O(2)–H---O(1') and O(2)–H---O(1). The adjacent molecules are connected through O(3)–H---O(4), N(3)–H---Cl(2) and N(3)–H---Cl(3) interactions to form a two dimensional supramolecular sheet extending parallel to  $[0\ 1\ 0]$  plane. The final  $R$ -value of complex 4 was 0.0333, and the final electrodensity map contains maximum and minimum peak heights of 0.581 and  $-0.500\ \text{e}\cdot\text{\AA}^{-3}$ , respectively.

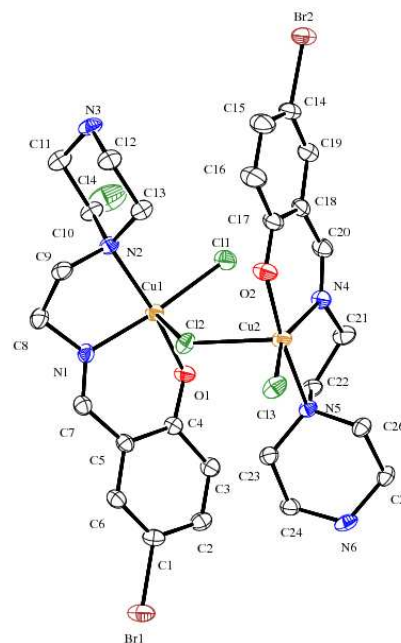


**Fig. 3** ORTEP representation of complex 8 showing an atom numbering scheme and displacement ellipsoid (30% probability level). All the hydrogen atoms are omitted for clarity.

### Description of crystal structure of $[(\text{CuL}^4\text{Cl})_2(\mu\text{-Cl})]\text{Cl}\cdot(\text{H}_2\text{O})_7$ , 8

Dark green crystals of complex  $[(\text{CuL}^4\text{Cl})_2(\mu\text{-Cl})]\text{Cl}\cdot(\text{H}_2\text{O})_7$ , 8 suitable for X-ray diffraction studies was obtained by the slow evaporation of reaction mixture for several weeks in dark room, which crystallizes in the monoclinic space group  $P2_1/n$ . Similar to complex 4, a chlorine atom forms bridge between the two copper atoms. The ORTEP representation of the molecule showing the numbering scheme is given in **Fig. 3**, while their selected bond lengths and angles are given in **Table S3**. The measured unit cell dimensions are  $a = 13.8391(4)$ ,  $b = 14.3968(4)$ ,  $c = 20.2234(7)$  Å,  $\beta = 98.6740(10)$  and  $Z = 4$ . The solved structure shows one chlorine atom bridges two mononuclear Cu(II) complexes through a 2-fold screw axis along  $[0, 1, 0]$  direction at  $(1/4, y, 1/4)$  with screw component  $[0, 1/2, 0]$  to form the dinuclear title complex. Apart from these, the structure contains one uncoordinated chlorine atom and seven water molecules occupy the crystal lattice as free molecules.

The copper(II) ions in complex 8 is pentacoordinated and the geometry around the copper nuclei is best described as square-pyramidal with a large contribution from the distortion constant (or) structural index parameter ( $\tau$ ) values of 0.002 and 0.335 for

Cu(1) and Cu(2), respectively ( $\tau = (\beta - \alpha)/60$ , where  $\beta$  and  $\alpha$  (in  $^\circ$ ) are the two largest L–M–L angles  $O(1)–Cu(1)–N(2) = 167.64(13)^\circ$ ;  $N(1)–Cu(1)–Cl(1) = 167.48(11)^\circ$ ;  $O(2)–Cu(2)–N(5) = 173.97(13)^\circ$ ;  $N(4)–Cu(2)–Cl(3) = 153.82(12)^\circ$ , a regular trigonal-bipyramid (TBP) and square-based pyramid (SP) have  $\tau$  values of 1 and 0, respectively).<sup>21</sup> The geometry and the bond distances/angles around the metal atoms Cu(1) and Cu(2) differ from each other. Among the two metal centers Cu(2) has comparatively larger distortion than the Cu(1) ion. The adopted five coordination geometry of the two metal ions consists of an imine [Cu(1)–N(1) = 1.955(3) and Cu(2)–N(4) = 1.964(3) Å] and piperazine nitrogen atoms [Cu(1)–N(2) = 2.104(3) and Cu(2)–N(5) = 2.089(3) Å], one phenolate oxygen atom [Cu(1)–O(1) = 1.945(3) and Cu(2)–O(2) = 1.935(3) Å] and a bridged chlorine atom [Cu(1)–Cl(2) = 2.626(12) and Cu(2)–Cl(2) = 2.524(12) Å] between the two metal ions, Cu(1) and Cu(2). The fifth coordination site of the metal ions is occupied by the chlorine atom at a distance of 2.270(12) and 2.325(12) Å for Cu(1)–Cl(1) and Cu(2)–Cl(3), respectively. As observed for complex **8**, the deprotonation of phenolic oxygen atom leads to shortening of C(4)–O(1) = 1.315(5), C(17)–O(2) = 1.310(5) Å bonds and the coordination of copper(II) atoms with O(1), O(2) leads to the lengthening of the C(3)–C(4) = 1.411(6), C(16)–C(17) = 1.411(6) Å and C(4)–C(5) = 1.419(6), C(17)–C(18) = 1.414(6) Å bonds compared to the bromophenol related Schiff base ligand.<sup>18</sup> The Cu(1)–Cu(2) distance of 4.612(8) Å and Cu(1)–Cl(2)–Cu(2) bond angle of 127.11(5) $^\circ$  is higher than that reported for the mono chloro-bridged Cu(II) complex [Cu(2)–Cu(3) = 4.016(2) Å and Cu(2)–Cl(2)–Cu(3) = 106.56(5) $^\circ$ ],<sup>22</sup> due to lesser bending angle. **Table S4** shows the hydrogen bonding parameters and **Fig. S2** shows the representation of intra- and inter molecular hydrogen bonding of complex **8**.

In complex **8**, the bond lengths around both metal atoms Cu(1) and Cu(2) are differ from each one. Cu(2) metal atom displays lesser bond lengths with phenolic oxygen (O1), piperazine nitrogen (N5) and bridged-chlorine (Cl2) atom whereas higher distance with imine nitrogen (N4) atom when compared to same with respect to Cu(1) metal atom. But both the metal atoms Cu(1) and Cu(2) exhibit lower coordination bond lengths with tridentate ligand and bridged-chlorine atoms than that of nickel atoms Ni(1) and Ni(2) of complex **4**, which implies the bond strength between metal and donor atoms.

### Electrochemical properties

The molar conductivity values in DMF solution ( $10^{-3}$  M) at 25  $^\circ$ C, for complexes **1–4** and **5–8** are in the range 282–294 and 125–137  $\Omega^{-1}$  cm<sup>2</sup> mol<sup>-1</sup>, due to tris-univalent and uni-univalent electrolytic behaviours, respectively.<sup>23</sup> The electrochemical properties of complexes have gained our attention because, the redox properties provides information for its further application in electrochemistry and catalytic reactions. Generally, the electrochemical properties of complexes depend on a number of factors such as chelation, axial ligation, degree and distribution of unsaturation and substitution pattern.<sup>24</sup> The redox behavior of all complexes has been investigated by cyclic voltammetry under similar experimental conditions.

The phenolic metal complexes usually undergo reduction at cathodic potentials, because of the negative influence and hard nature of phenoxide atoms in the ligand.<sup>25</sup> The complex structure

and the nature of the substituents at *para* position of the phenoxide ion in benzene ring influences the redox behavior in the negative potential range. Reduction process voltammograms for complexes **1–8** are shown in **Fig. S3 & S4** and the results are given in **Table S5**.

In cathodic region, all complexes show two reduction waves at different potentials. From the voltammograms,  $\Delta E_p$  value for the Ni(II) complexes for the first and second redox couple are more than 500 and 400 mV, respectively. This higher  $\Delta E_p$  value is due to the difference between the original complex and the reduced species. The cyclic voltammograms of Ni(II) and Cu(II) complexes show the first reduction potential values in the following order  $[ML^3]_2 > [ML^4]_2 > [ML^1]_2 > [ML^2]_2$ . The observed less negative potential of the first reduction process for complexes containing ligands  $L^{3\&4}$ , when compared to other complexes is due to the presence of electron withdrawing substituent at the *para* position of phenoxide ion in the phenyl ring and reduced at less negative potential, which decreases the electron density around the metal ions and favors easy reduction.

Based on the observations, the reduction processes for Ni(II) and Cu(II) complexes are irreversible. The following steps may involve in the reduction process:



The cyclic voltammograms of oxidation process for Ni(II) complexes **1–4** are shown in **Fig. S5** and the oxidation peak values are given in **Table S5**. The nature of the oxidation process is quasi-reversible and the following steps may involve in the oxidation process:



When compared to the chloro complex, the bromo complex gives higher values of  $E^1_{1/2}$  and  $E^2_{1/2}$ . This is due to the addition of an electron to the bromo complex is more difficult than the chloro complex as the basicity of the bromide ion is higher when compared to the chloride ion.

### Determination of stability constants and thermodynamic parameters

The stability constants ( $\ln K$ ) of the selected complexes in 90% aqueous DMF were determined at different ionic strengths ( $I = 0.05, 0.10$  &  $0.20$ ) and temperatures (25, 35 &  $45 \pm 0.2$   $^\circ$ C) using a spectrophotometric method. It was found that the stability constant value of the complexes is proportional to the ionic strength and inversely proportional to the temperature (**Table 1**). Thermodynamic stability constants ( $\ln K^\circ$ ) and thermodynamic parameters ( $\Delta H^\circ$ ,  $\Delta S^\circ$  &  $\Delta G^\circ$ ) of the complexes were derived from the stability constants.<sup>26</sup> The plots of  $\ln K^\circ$  versus  $1/T$  at zero ionic strength gave linear curves (**Fig. 4**), showing that  $\Delta H^\circ$  and  $\Delta S^\circ$  are essentially independent of temperature over the temperature range considered. The  $\Delta H^\circ$  and  $\Delta S^\circ$  values were calculated from the plots ( $-\Delta H^\circ/R =$  slope and  $\Delta S^\circ/R =$  intercept, at  $1/T = 0$ ). The value of  $\Delta G^\circ$  was calculated for each metal–ligand system by using the following equation,  $\Delta G^\circ = -RT \ln K^\circ$ . The results of thermodynamic parameters implies the exothermic nature ( $-\Delta H^\circ$ ) of the metal–ligand interaction, and spontaneous ( $+\Delta S^\circ$  &  $-\Delta G^\circ$ ) formation of the complexes.

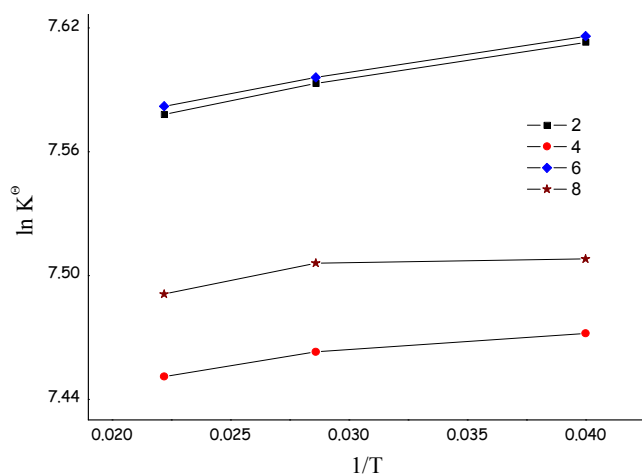


**Fig. 4** The plot of thermodynamic stability constant of complexes **2**, **4**, **6** and **8** versus  $1/T$ .

**Table 1** The stability constants ( $\ln K$ ) at different temperatures and ionic strengths ( $I = \text{mol/dm}^3$ ), and the thermodynamic parameters

Complex	Temp K	$\ln K$			$\ln K^\circ$	$-\Delta G^\circ/kJ/mol$	$-\Delta H^\circ/kJ/mol$	$\Delta S^\circ/J/mol K$
		$I = 0.20$	$I = 0.10$	$I = 0.05$				
<b>2</b>	298	7.660	7.636	7.625	7.613	18.86		
	308	7.617	7.605	7.599	7.593	19.44	17.86	
	318	7.612	7.595	7.586	7.578	20.04		
<b>4</b>	298	7.496	7.486	7.478	7.472	18.51		
	308	7.485	7.474	7.469	7.463	19.11	9.11	
	318	7.474	7.463	7.456	7.451	19.70		
<b>6</b>	298	7.628	7.622	7.619	7.616	18.87		
	308	7.633	7.616	7.604	7.596	19.45	18.71	
	318	7.629	7.601	7.595	7.582	20.05		
<b>8</b>	298	7.606	7.555	7.534	7.508	18.60		
	308	7.566	7.536	7.522	7.506	19.22	9.59	
	318	7.575	7.530	7.513	7.491	19.81		

5

### Magnetic properties

**EPR and VSM studies:** The  $3d^9$  configuration of Cu(II) with square-pyramidal geometry have magnetic moment approximately given by the spin-only value of  $\sqrt{3}\mu_B$ . The room temperature magnetic moment ( $\mu_{\text{eff}}$ ) values for the chloro-bridged copper(II) complexes **5–8** were calculated by the equation,  $\mu_{\text{eff}} = 2.828[\chi_M T]^{1/2}$  and ranges from 1.49 to 1.52 BM, which is lower than the spin-only value of 1.73 BM for high spin Cu(II) center with  $S = 1/2$ , suggests the presence of intramolecular antiferromagnetic interaction between Cu(II) nuclei. X-band EPR spectra of all the dry and powdered copper(II) complexes exhibit a broad signal (Fig. S6) with  $g_{\parallel}$  value 2.15–2.19, and the similar results obtained in DMF solution implies that the square-pyramidal geometries of the complexes, as observed in the X-ray crystal structure of complex **8**, is retained in solution.

Temperature-dependent magnetic susceptibilities of dry and powdered complexes **5–8** were measured in the temperature

range 20–300 K at a constant applied magnetic field of 5000 Oe. The results of the magnetic measurements for complex **8** is displayed in terms of molar susceptibility ( $\chi_M$ ), effective magnetic moment ( $\mu_{\text{eff}}$ ), and  $\chi_M T$  product versus thermal variation in Fig. 6. The molar susceptibility  $\chi_M$  value increases smoothly from  $0.9 \times 10^{-3} \text{ cm}^3 \text{ mol}^{-1}$  with decrease in temperature from 300 K, and between 80 to 20 K a rapid increase from  $2.5 \times 10^{-3} \text{ cm}^3 \text{ mol}^{-1}$  to  $9 \times 10^{-3} \text{ cm}^3 \text{ mol}^{-1}$  is observed. The change of magnetic moment with temperature in the dinuclear copper(II) complexes usually supported by the following factors: contribution of orbital momentum, intramolecular magnetic interaction between two metal centers and antiferromagnetic interaction.<sup>27</sup> The effective magnetic moment of complex **8** decreases slowly from  $1.50 \mu_B$  at 300 K to  $1.35 \mu_B$  at 60 K and then decreases rapidly to  $1.18 \mu_B$  at 20 K indicating strong intramolecular antiferromagnetic exchange interaction between two Cu(II) nuclei. As T lowers from 300 to 55 K, the  $\chi_M T$  product of **8** decreases monotonously from 0.28 to  $0.22 \text{ cm}^3 \text{ K mol}^{-1}$  and then rapid decrease to  $0.18 \text{ cm}^3 \text{ K mol}^{-1}$  at 20 K, due to temperature-independent paramagnetism. The observed behavior suggests the existence of an intramolecular antiferromagnetic interaction between copper(II) centers. The susceptibility data were least-squares fitted to the modified Bleaney-Bowers equation for Cu(II) dimers.<sup>28</sup>

$$\chi_M = Ng^2\beta^2/3kT[(1-P)(3+e^{-2J/kT})^{-1}] + 0.45(P/T) + N_a$$

Where,  $\chi_M$  – molar magnetic susceptibility;  $N$  – Avogadro's number;  $g$  – average gyromagnetic ratio fixed at 2.18 obtained from EPR measurements;  $\beta$  – Bohr magneton;  $k$  – Boltzmann constant;  $J$  – singlet-triplet energy separation;  $P$  – percentage of monomeric impurities (0.0015);  $N_a$  – temperature independent paramagnetism (TIP) usually assumed to be  $120 \times 10^{-6} \text{ cm}^3 \text{ mol}^{-1}$  for Cu(II) dimers. From the best fit of Bleaney-Bowers equation, the singlet-triplet energy separation,  $-2J$ , is calculated to be  $228 \text{ cm}^{-1}$  at room temperature. The obtained  $-2J$  value and increase of  $\chi_M$ , the decrease of  $\mu_{\text{eff}}$  and  $\chi_M T$  product upon lowering the temperature suggest the presence of an intramolecular antiferromagnetic interaction between the two Cu(II) centers via chloride-bridge. The observed lower  $-2J$  value for complexes **7** ( $220 \text{ cm}^{-1}$ ) and **8** ( $228 \text{ cm}^{-1}$ ), when compared to complexes **5**

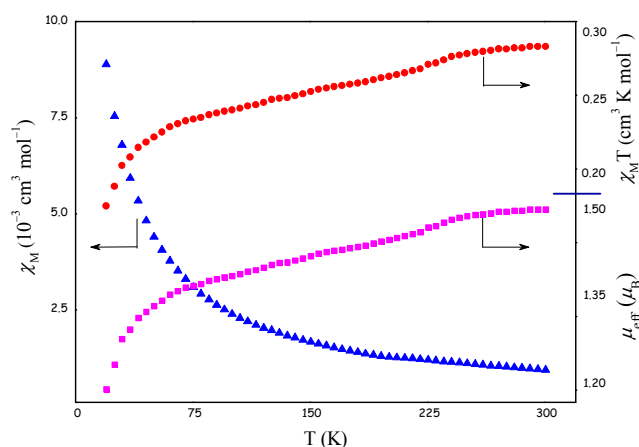


**Fig. 5** Temperature dependence of  $\chi_M$ ,  $\mu_{\text{eff}}$  and  $\chi_M T$  product for complex **8** in the range 20–300 K.

(236  $\text{cm}^{-1}$ ) and **6** (239  $\text{cm}^{-1}$ ) is due to the presence of electron withdrawing substituents on the phenyl ring which decreases the electron density on the copper(II) nuclei *i.e.* reduction in electron density on the copper nuclei are less favorable for effective coupling resulting in a lower  $-2J$  value.<sup>29</sup>

**Magneto-structural correlation:** The strong antiferromagnetic interaction can be explained as follows: The magneto-structural parameters of complex **8** are compiled and the results are consistent with those of related mono chloro-bridged complexes.<sup>30</sup> In a square-pyramidal geometry around the Cu(II) ions, the unpaired electron mainly resides in the  $d_{x^2-y^2}$  orbital *i.e.* magnetic orbital, and a half-filled band formed by combination of such orbitals correspond to the highest occupied band (HOB). The two copper(II) nuclei have a square-pyramidal geometry with an apices occupied by the bridged-chlorine for both Cu(1) and Cu(2), coupling can occur through this chloro-bridge. In a series of mono chloro-bridged copper(II) dimeric complexes, Hatfield *et al.*<sup>31</sup> has suggested that a smooth correlation exists between the exchange parameter  $J$  and the ratio  $\theta/R$  (where  $\theta$  is the magnitude of the angle at the Cu(1)–Cl–Cu(2) bridge and  $R$  is the Cu–Cl distance). The overall magnetic behaviour can be expected for values of the quotient  $\theta/R$  lower than approximately 40 and higher than 57 while antiferromagnetic character appears when this quotient  $\theta/R$  is between these two values. Cortés *et al.*<sup>32</sup> have reported that the increase in distortion of square-pyramidal toward the trigonal bipyramidal geometry causes an effective mixing of magnetic orbitals with the  $d_{z^2}$  orbital and leads to stronger magnetic interactions and also observed an increase in antiferromagnetic coupling as the Cu–Cl–Cu angle increases. The increase in distance between metal centers influencing the exchange parameter  $J$  which becomes more negative. Thus, the observed  $-2J$  value ( $-228 \text{ cm}^{-1}$ ) found for chloro-bridged copper(II) complex **8** can be explained by the presence of a relatively higher Cu(1)–Cl(2)–Cu(2) angle of  $217.11(5)^\circ$  and less Cu(1)–Cu(2) distance of  $3.954 \text{ \AA}$ .<sup>33</sup>

#### Antioxidant studies

Many bioorganic redox processes generate free radicals such as superoxide anion radical ( $\text{O}_2^-$ ) and hydroxyl radical ( $\text{OH}^\cdot$ ) that may induce oxidative damage in various components of the body (lipids, proteins and DNA) and have been implicated in aging and a number of life-limiting chronic diseases (cancer, hypertension, cardiac infarction, atherosclerosis, rheumatism, cataracts, etc.).<sup>34</sup> Efforts to counteract the damage caused by these species are gaining acceptance as a basis for novel therapeutic approaches and the field of preventive medicine is experiencing an upsurge of interest in useful antioxidants. The hydroxyl radical is by far the most potent and therefore the most dangerous oxygen metabolite, elimination of this radical is one of the major aims of antioxidant administration. DPPH assay is widely used for assessing the ability of radical scavenging activity and it is measured in terms of  $\text{IC}_{50}$  values. The hydroxyl radical in aqueous media was generated by the Fenton system. To explore the DPPH radical scavenging ability of the newly synthesized dinuclear complexes, we have carried out the experiments with the hope of developing potential antioxidants and therapeutic agents for certain chronic diseases.

The DPPH radical is a stable free radical which shows a strong absorption band at 517 nm in visible spectrum due to the presence of an odd electron. As this electron becomes paired off in the presence of a free radical scavenger, this absorption vanishes resulting in decolorization stoichiometrically with respect to the number of electrons taken up. The reactivity of free radicals can be neutralized by the donation of an electron or hydrogen. Lower the  $\text{IC}_{50}$  values, greater the hydrogen donating ability and thus the antioxidant activity of the free radical scavengers. We have compared the abilities of the present complexes to scavenge DPPH radicals with those of the well-known standards including natural antioxidant vitamin C and synthetic antioxidant BHT (Butylated toluene) under the same experimental conditions. The  $\text{IC}_{50}$  values (Table 2) obtained from *in vitro* radical scavenging assay strongly support that complexes presented in this work possess excellent scavenging activity against DPPH radical, which is more or less equal to the standard antioxidants (vitamin C and BHT). Among these tested complexes, copper(II) complexes show better scavenging activity than nickel(II) analogous, because of the availability of an odd electron in copper(II) ion, which decreases the capacity to stabilize unpaired electrons and there by arrest the free radicals. The antioxidant efficacy ( $\text{IC}_{50}$ ) of the present complexes decreases in the order of **6** ( $85.3 \pm 1.6$ ) > **5** ( $88.1 \pm 0.9$ ) > **8** ( $92.9 \pm 4.8$ ) > **7** ( $95.8 \pm 3.3$ ) > **2** ( $124.1 \pm 1.2$ ) > **1** ( $131.8 \pm 3.6$ ) > **4** ( $166.3 \pm 1.4$ ) > **3** ( $186.5 \pm 0.9$ ). The scavenging effects of the copper(II) complexes is significantly higher than that of nickel(II) complexes containing the same ligands. These results clearly indicate that the synergic combination of ligand and metal ions plays vital role in the design of a potential antioxidant. The antioxidant property of different ligands follows the same order by changing metal ions. The presence of an electron releasing group at the *para* position to the phenoxo-ligand shows higher radical scavenging activity than that with an electron withdrawing group. Although the mechanism of radical scavenging activity of complexes under study remains unclear, these experimental results are helpful in designing more effective antioxidant agents against DPPH radical and also other free radicals.

**Table 2** *In vitro* antioxidant and cytotoxicity assays for complexes

Complexes	$\text{IC}_{50} \pm \text{SD}$ ( $\mu\text{M}$ ), DPPH	$\text{IC}_{50} \pm \text{SD}$ ( $\mu\text{M}$ ), HepG2		Comet assay score (%)
		24 h	48 h	
1	$131.8 \pm 3.6$	-	-	-
2	$124.1 \pm 1.2$	$18.7 \pm 0.3$	$5.4 \pm 0.7$	64.99
3	$186.5 \pm 0.9$	-	-	-
4	$166.3 \pm 1.4$	-	-	-
5	$88.1 \pm 0.9$	-	-	-
6	$85.3 \pm 1.6$	$9.3 \pm 0.4$	$2.3 \pm 0.6$	82.12
7	$95.8 \pm 3.3$	-	-	-
8	$92.9 \pm 4.8$	$15.6 \pm 1.1$	$3.9 \pm 0.5$	73.38
Vitamin C	$144.6 \pm 1.8$	-	-	-
BHT	$91.4 \pm 3.1$	-	-	-
Cisplatin	-	$10.2 \pm 0.5$	$2.5 \pm 0.3$	-

### DNA binding studies

Biological investigations have been performed in Tris-HCl/NaCl buffer, so it was necessary to check the stability of complexes (1–8) in this buffer. A negligible absorbance and current change was observed after 48 h in electronic spectra and cyclic voltammetry, respectively. Little absorbance/current change without any considerable shift in wavelength/potential predicted the stability of complexes in this buffer.

**Absorption spectral titration:** In order to investigate the possible binding mode and propensity of the molecules to CT-DNA, various techniques are studied. Electronic absorption spectroscopy is one of the most widely used techniques to follow the interaction of metal complexes with DNA. Literature data usually takes place through both covalent (*via* replacement of a labile group of complex by a nitrogen donor atom from the

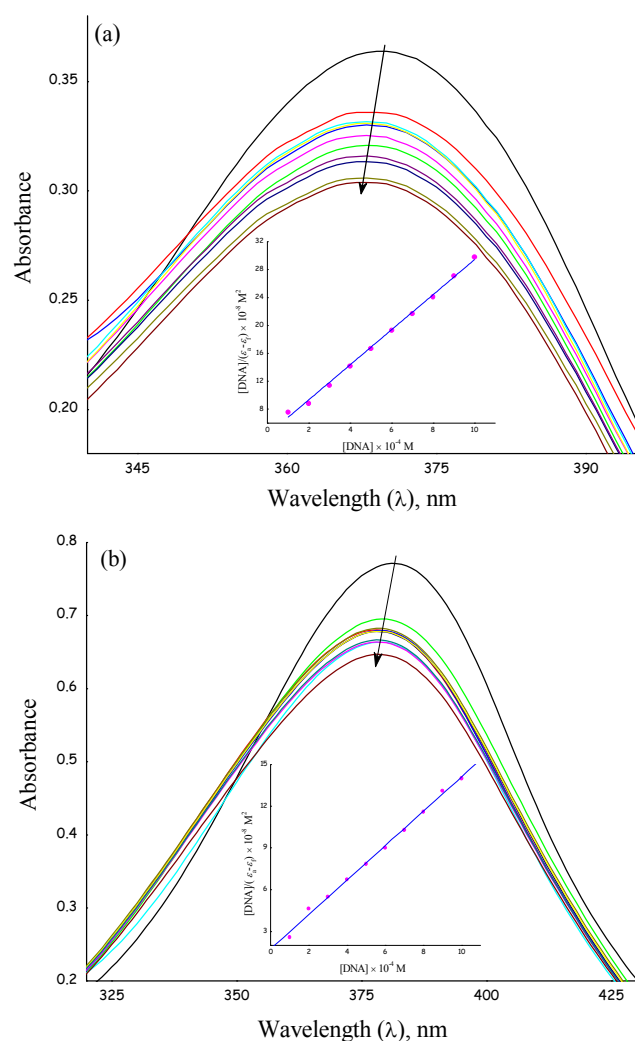


**Fig. 6** Absorption spectra of complexes 4 (a) & 7 (b) (50  $\mu\text{M}$ ) in Tris-HCl/NaCl (pH 7.2) buffer upon addition of CT-DNA (0–500  $\mu\text{M}$ ). Arrow shows the decrease in absorbance upon increasing concentration of DNA. Inset: Plot of  $[\text{DNA}]/(\epsilon_a - \epsilon_t)$  vs  $[\text{DNA}]$  for absorption titration of CT-DNA with complexes.

nucleotide of DNA such as guanine N7) and/or non-covalent (intercalative, electrostatic and surface (major/minor groove) binding) interaction. In general, hypochromism and hyperchromism are the known spectral changes typical of metal complexes associated with DNA helices.

The hyperchromic effect is due to surface binding while the hypochromism accompanied by a significant red/blue shift is characteristic of strong  $\pi$ - $\pi$  stacking interaction between the aromatic chromophore ligand of a metal complex and the aromatic rings of DNA bases with the extent of hypochromism commonly consistent with the strength of intercalation.<sup>35</sup> The  $\pi^*$  orbital of intercalated ligand of a complex is coupled with the  $\pi$  orbital of DNA bases. This coupling results in decreasing  $\pi$ - $\pi^*$  transition energy and bathochromism is observed. The coupling  $\pi$  orbitals, which are also partially filled by electrons, lowers the transition probability and concomitantly results in hypochromism.<sup>36</sup>

**Fig. 6** shows the absorption spectra of complexes 4 & 7 in the absence and presence of CT-DNA (for other complexes, the spectra are shown in **Fig. S7–S9**), and the resulting data is summarized in **Table 3**. Upon increasing the CT-DNA concentration, UV-Vis spectra of complex-DNA solutions clearly show the tendency of hypochromism with blue shift. The observed changes in the absorption bands of complexes 1–8 at a ratio ( $R$ ) of  $[\text{DNA}]/[\text{complex}] = 10$ , unambiguously revealed the intercalative binding mode of complexes with CT-DNA.<sup>37</sup> The presence of cationic charge on the coordination sphere would lead to electrostatic interaction with the negatively charged phosphate group in the backbone of the DNA. Additionally, hydrogen bonding is also possible in the interaction of DNA with complexes. DNA possesses several hydrogen bonding sites in the major as well as minor grooves. Since, complexes 1–8 contains  $-\text{NH}$  groups, there could be hydrogen bonding between complexes and base pairs in DNA.<sup>38</sup> However, the hydrogen bonding is a weak interaction. The observed decrease in the order of hypochromism reflects the decrease in DNA binding affinities of complexes in the same order. To compare the binding affinities of complexes to DNA quantitatively, the intrinsic binding constant  $K_b$  of complexes 1–8 are calculated and found in the range  $1.56 (\pm 0.6) - 1.96 (\pm 0.4) \times 10^4 \text{ M}^{-1}$ . The binding strength of complexes are more or less equal to the binding strength of the previously reported dinuclear complexes,<sup>39</sup> and lower than that of the reported classical intercalators (EtBr, in Tris-HCl/NaCl buffer (25:40), pH 7.9 and  $[\text{Ru}(\text{phen})_2(\text{dppz})]^{2+}$ ), in which the binding constants have been found to be in the order of  $10^6 - 10^7 \text{ M}^{-1}$ .<sup>40</sup>

Hence from the obtained results, it has been found that the copper(II) complexes exhibit higher binding affinity with CT-DNA than the nickel(II) complexes and, the binding strength of complexes decreases in the order  $6 > 5 > 7 > 8 > 2 > 1 > 3 > 4$ . The obtained higher hypochromism and  $K_b$  value for complex 6 (Complex 2 in the case of nickel(II) analogues) suggest its higher binding affinity to DNA than that for other complexes. This may be due to the presence of methyl group on the phenyl ring, which is involved in hydrophobic interaction with the hydrophobic DNA surface that leads to the enhancement of DNA binding affinity. Overall, the binding constant values imply the medium binding strength of the dinuclear complexes with CT-DNA.

75

**Table 3** Absorption spectral properties of complexes 1–8 bound to CT-DNA

Complexes	$\lambda/\text{nm}$	$R$	Change in Absorption	$\Delta\lambda/\text{nm}$	$^aH\%$	$K_b \pm \text{SD} (10^4 \text{ M}^{-1})$
1	372	10	Hypochromism	6	18	$1.68 \pm \sim 0.4$
2	381	10	Hypochromism	3	20	$1.76 \pm \sim 0.3$
3	382	10	Hypochromism	4	17	$1.62 \pm \sim 0.7$
4	369	10	Hypochromism	3	15	$1.56 \pm \sim 0.6$
5	359	10	Hypochromism	12	24	$1.85 \pm \sim 0.9$
6	358	10	Hypochromism	4	31	$1.96 \pm \sim 0.4$
7	358	10	Hypochromism	6	24	$1.83 \pm \sim 0.5$
8	372	10	Hypochromism	8	21	$1.77 \pm \sim 0.3$

$$^aH\% = [(A_{\text{free}} - A_{\text{bound}}) / A_{\text{free}}] \times 100\%$$

Measurements were made at  $R = 10$ , where  $R = [\text{DNA}] / [\text{Complex}]$ ;  $[\text{DNA}] = 0\text{--}500 \mu\text{M}$ ;  $[\text{Complex}] = 50 \mu\text{M}$ .  $\sim$  shows the decimal ( $\pm 0.05$ ) difference in the results.

**Hydrodynamic (Viscosity) measurements:** To further investigate the binding mode and binding intensity of complexes with DNA, the DNA viscosity variance at 25 °C was studied by changing the concentration of complexes. Viscosity of DNA is sensitive to its length. Intercalating agents are expected to elongate the double helix to accommodate the ligands in between the base leading to an increase in the viscosity of DNA. In contrast, a partial/non-classical intercalation of ligand may provoke a bend or kink the DNA helix, reduce its effective length and concomitantly viscosity, whereas groove or electrostatic mode of binding cause little or no effect on the relative viscosity of DNA solution. Therefore viscosity measurements are regarded as the least ambiguous and most critical means of studying the binding mode of metal complexes with DNA in solution and provide stronger arguments for an intercalation mode of binding.<sup>41,42</sup> The values of relative specific viscosity ( $\eta/\eta_0$ ), where  $\eta$  and  $\eta_0$  are the specific viscosities of DNA in the presence and absence of complex, are plotted against  $1/R$  ( $[\text{Complex}]/[\text{DNA}] = 0.05\text{--}0.5$ ).

Ethidium bromide (EtBr) usually increases the relative viscosity due the lengthening of DNA double helix, which results from intercalation. Upon increasing amount of complexes 1–8, the obtained plot shows only a minor change in relative viscosity of DNA (Fig. S10), which indicates groove or electrostatic interaction along with partial intercalative mode of binding between DNA base pairs and each complex. Furthermore, the cationic complexes would interact with the polyanionic backbone of DNA, which supports the possible of electrostatic interaction between DNA and complexes. The binding ability of complexes varies in the order  $6 > 5 > 7 > 8 > 2 > 1 > 3 > 4$ . Thus, complexes show an increase in viscosity, which is lower than that for the classical intercalator EtBr.<sup>43</sup> The highest increase in DNA viscosity was effected by complex 6, suggesting that complex dramatically increase the hydrodynamic length of DNA as a consequence of the untwisting of the base pairs and helical backbone of DNA needed to accommodate the intercalators.<sup>44</sup> The results were in accordance with UV-Vis absorption spectral results.

**Electrochemical titration:** The metal complexes of high oxidation state play an important role in bioinorganic chemistry, because of their biological significance as redox enzyme models. To further explore the interaction mode between complexes and

DNA, cyclic voltammetry was used which is considered to be a very sensitive analytical technique to determine changes in redox behaviour of metallic species in the presence of bio-molecules. The electrochemical investigations of metal-DNA interaction can provide a useful complement to spectroscopic methods and

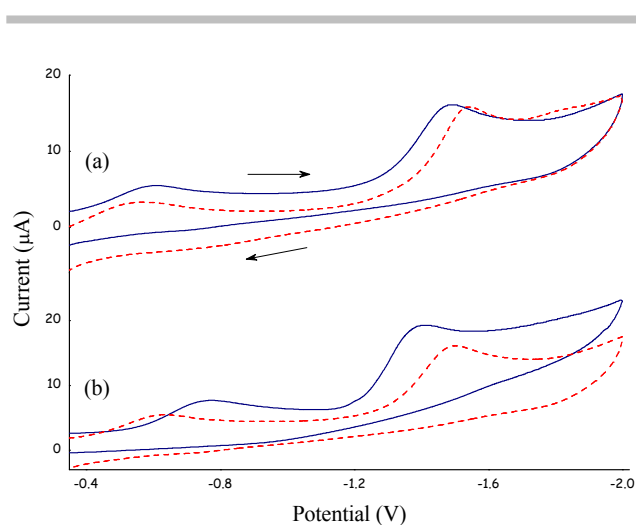


**Fig. 7** Cyclic voltammograms of complexes 2 (a) & 6 (b) in the absence (solid line) and presence of CT-DNA (dotted line).  $[\text{Complex}] = [\text{DNA}] = 100 \mu\text{M}$  and, scan rate was  $100 \text{ mVs}^{-1}$ .

viscometric studies (e.g. for non-absorbing species, and yield information about interaction with both the reduced and oxidized form of the metal ion).<sup>45</sup> In general, when the redox active metal complex binds to DNA *via* intercalation, the potential presents a positive shift, while in the case of electrostatic interaction, the potential will shift to a negative direction. If more than one potential exist simultaneously, a positive and negative shift of  $E_p^1$  and  $E_p^2$ , respectively, the molecule can bind to DNA by both intercalation and electrostatic interaction.<sup>40</sup>

Since complexes 1–8 possess redox active moieties, their electrochemical properties are expected to be altered in the presence of DNA which can be followed by CV studies. On the incremental addition of CT-DNA ( $R = [\text{DNA}]/[\text{Complex}]$ ) to the metal complexes, no new reduction waves (Fig. 7) appeared and the observed decrease in current intensity is due to the diffusion of the equilibrium mixture of free and DNA-bound complex to the electrode surface which suggest the existence of same electrochemical behaviour upon addition of CT-DNA. The significant drop of cathodic peak current on the addition of DNA is observed *i.e.* the value of  $i_{pc}$  decreases regularly with increase in DNA concentration. The slower mass transfer of complexes bound to DNA fragments leads to a decrease in concentration of the unbound redox-active species in solution. The decrease in voltammetric current with positive ( $E_p^1$ ) and negative ( $E_p^2$ ) potential shifts suggests the possible existence of intercalation along with electrostatic mode of interaction of complexes with DNA.<sup>40,46</sup> The decrease in peak current is much higher for copper(II) complexes than for nickel(II) complexes upon addition of DNA which suggest the stronger binding affinity of the former to DNA than that of later and follows the order  $6 > 5 > 7 > 8 > 2$

> **1** > **3** > **4**. The electrochemical studies corroborated well with the electronic absorption studies and thereby authenticate the strong interaction of CT-DNA with complexes **1–8**.

### Nuclease activity

The degradation of plasmid DNA explored by transition metal complexes has been interest of researchers. This can be achieved by targeting the basic components of DNA such as phosphodiester linkages, deoxyribose sugar or nucleobases. The nuclease activity of complexes **1–8** have been studied using supercoiled (SC) pBR322 DNA (33.3  $\mu$ M) as a substrate in a medium of Tris-HCl/NaCl (pH 7.2) buffer at 37  $^{\circ}$ C by gel electrophoresis, in which the transition from the naturally occurring, covalently closed circular form to the open circular form and linear form was monitored. The migration of DNA in gel electrophoresis works under the influence of electric potential. DNA is negatively charged species, when placed under electric field, it will migrates toward anode and this migration depends on the size of DNA, electric field strength, gel density and the buffer nature. When circular pBR322 DNA is subjected to electrophoresis, relatively fast migration will be observed for the intact supercoiled form (Form I). If scission occurs on one strand (nicking), the supercoiled form will relax to generate a slower-moving nicked form (Form II). If both strands are cleaved, a linear form (Form III) that migrates between Form I and Form II will be generated. The observed results show appreciable nuclease activity by the copper(II) complexes (**5–8**) when compared to nickel(II) analogues (**1–4**) and no cleavage was observed for controls both in the absence and presence of  $H_2O_2$ . The appearance of electrophoresis band characteristic of nicked circular form (NC, Form II) and the absence of a band corresponding to linear circular form (LC, Form III) suggest that only single-strand DNA cleavage occurs for complexes.

**Nuclease activity in the absence of  $H_2O_2$ :** In general, the Ni(II) and Cu(II) complexes cleave DNA by hydrolytic pathway.<sup>47</sup> Since the synthesized complexes satisfies one of the primary criteria for catalyzing hydrolytic cleavage of DNA, *i.e.* coordination of the phosphate moiety of DNA to the metal(II) center of complex, its DNA cleaving ability has been investigated with different concentration of complexes. The nuclease activity of complexes was observed in the absence of external agents and the increasing intensity of NC form was found with increase in

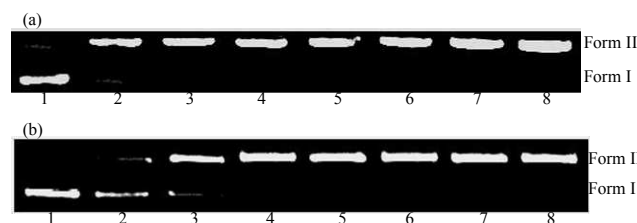


**Fig. 8** Hydrolytic cleavage of pBR322 DNA (33.3  $\mu$ M) by complexes **6** (a) and **8** (b) in 5 mM Tris-HCl/50 mM NaCl buffer (pH 7.2). Lane 1, DNA alone; lane 2, DNA + **6/8** (25  $\mu$ M); lane 3, DNA + **6/8** (50  $\mu$ M); lane 4, DNA + **6/8** (75  $\mu$ M); lane 5, DNA + **6/8** (100  $\mu$ M); lane 6, DNA + **6/8** (150  $\mu$ M); lane 7, DNA + **6/8** (200  $\mu$ M); lane 8, DNA + **6/8** (250  $\mu$ M).

concentration of complexes. The copper(II) complexes shows (Fig. 8) prominent DNA cleavage to give nicked circular (NC) form (> 75%), while nickel(II) complexes (Fig. S11) fail to show the expected efficiency (< 35%).

From the obtained results and literature reports,<sup>48,49</sup> the following interaction was concluded between metal ions and phosphate moiety of DNA. The metal(II) ions may bind with the phospho-diester bond of DNA through the coordinate linkage and/or electrostatic interaction, and the metal ions activate the central phosphorus atom of DNA, resulting in the formation of five coordinated phosphorus intermediate. Then, the activated phosphorus atom is attacked nucleophilically by the metal ions due to their Lewis acidity *via* charge neutralization, and finally one of the P–O ester bond of nucleic acid is cleaved.

The presence of more aromatic moiety and hard Lewis acid properties could play a vital role in the DNA cleavage process by hydrolytic pathway.<sup>49</sup> The potency of the dinuclear complexes in nuclease activity follows the order **6** > **5** > **7** > **8** > **2** > **1** > **3** > **4**. The difference in nuclease activity of complexes may be due to the influence of the substituted groups in complexes, which makes it interact with DNA more effectively. The cleavage ability of complexes might be due to the binding affinity of complexes with DNA, and the cleavage of DNA by complex is dependent on the concentration of complexes. To ascertain the hydrolytic cleavage mechanism, an additional cleavage experiments were conducted using enzymatic T4 ligase assay. The cleavage product of SC form by complexes, reacted with T4 ligase enzyme and result implies that 10–20% nicked form moves to SC form *i.e.* nicked circular form religated to closed circular and then supercoiled form. The observed result of T4 ligase enzymatic assay reveals the hydrolytic DNA breakage mechanism.

**Nuclease activity in the presence of  $H_2O_2$ :** The damage of plasmid DNA is also dependent on co-oxidant used. As shown in Fig. 9, in the presence of  $H_2O_2$ , the degradation of supercoiled Form I to nicked Form II is induced by complexes, in which the copper(II) complexes exhibit pronounced cleavage activity than

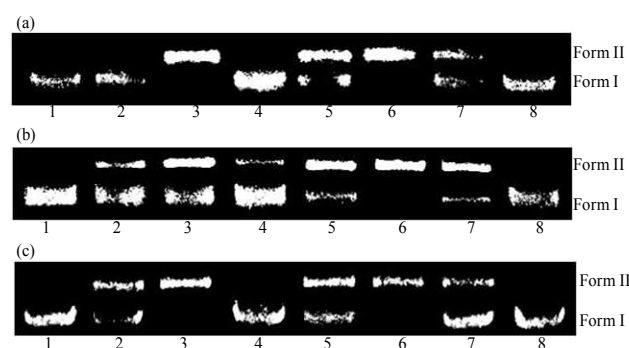


**Fig. 9** Oxidative cleavage of pBR322 DNA (33.3  $\mu$ M) by complexes **5** (a), **6** (b) and **8** (c) in the presence of  $H_2O_2$  (40  $\mu$ M) and DMSO (0.2 mM) in 5 mM Tris-HCl/50 mM NaCl buffer (pH 7.2). Lane 1, DNA control; lane 2, DNA + **5/6/8** (100  $\mu$ M); lane 3, DNA + **5/6/8** (100  $\mu$ M) +  $H_2O_2$ ; lane 4, DNA + **5/6/8** (100  $\mu$ M) +  $H_2O_2$  + DMSO; lane 5, DNA + **5/6/8** (200  $\mu$ M); lane 6, DNA + **5/6/8** (200  $\mu$ M) +  $H_2O_2$ ; lane 7, DNA + **5/6/8** (200  $\mu$ M) +  $H_2O_2$  + DMSO; lane 8, DNA +  $H_2O_2$  + DMSO.

the nickel(II) analogues. The oxidative cleavage mechanism was proposed as follows: When redox-active metal complexes interact with DNA in the presence of a co-oxidant, it is believed to produce different oxygen intermediates (reactive oxygen species), depending on specific complex and conditions. A non-diffusible metal-peroxo intermediate has been invoked in some cleavage reactions while in others, Fenton-like chemistry, which invokes release of freely diffusible hydroxyl (OH<sup>•</sup>) or hydroperoxyl (HO<sub>2</sub><sup>•</sup>) radical, has been assumed. The metal complexes in the presence of H<sub>2</sub>O<sub>2</sub> may generate reactive hydroxyl/hydroperoxyl radical that can damage the deoxyribose ring (C3'), or alternatively a metal-peroxo species may participate directly in the oxidation of deoxyribose ring.

To understand the involvement of reactive oxygen species (ROS), inhibition experiment was carried out with standard scavengers of reactive oxygen intermediates in the electrophoresis studies under physiological conditions. DMSO has little influence on DNA cleavage, suggesting that the hydroxyl radical is involved in the DNA scission process. A possible hydroxyl radical based cleavage reaction is shown in **Scheme S1**. In addition, the coordination environment of the central metal ions and geometry of complexes not only governs the DNA binding but also determine the nucleolytic action. Therefore, the difference in nuclease activity of complexes may be attributed to their proximity to DNA binding. The nuclease activity of redox mediated or photo activated metal complexes is an important element in the characterization of DNA recognition of transition metal complexes.

#### Growth inhibition activities

**Cell viability analysis:** Hydrolysis of DNA *via* phospho-diester bond is crucial at several stages in the cell cycle, including DNA repair and excision, integration and signal transduction.<sup>49</sup> Meanwhile, damage of DNA backbone by hydrolytically has been reported to be related to antitumor potential,<sup>50</sup> which prompts us to evaluate cytotoxicity of complexes. The toxicity of the complexes was examined against non-cancer cell line (Vero cell line), and the obtained results show that the negligible toxicity level (5-14%) of the complexes against the non-cancer cell line. *In vitro* cytotoxicity of the chloro-bridged dinuclear nickel(II) complex **2** and copper(II) complexes **6** and **8** against human hepatocellular liver carcinoma cell line HepG2 have been investigated in comparison with the widely used drug, cisplatin under identical conditions, by MTT reduction assay. The assay is based on the fact that only live cells reduce yellow MTT but not dead cells to blue farmazone products. Thus, the metabolic activity of the cells was assessed by their ability to cleave the tetrazolium rings of pale yellow MTT and form a water-insoluble dark blue farmazone crystal. Assay shows that complexes inhibit the growth of cells. The IC<sub>50</sub> values (**Fig. 10**, **Table 2**) for 48 h incubation are lower than those for 24 h incubation and IC<sub>50</sub> values decreases with increasing concentration of complexes, which clearly indicating that the cytotoxicity of dinuclear complexes are dose and time dependent.

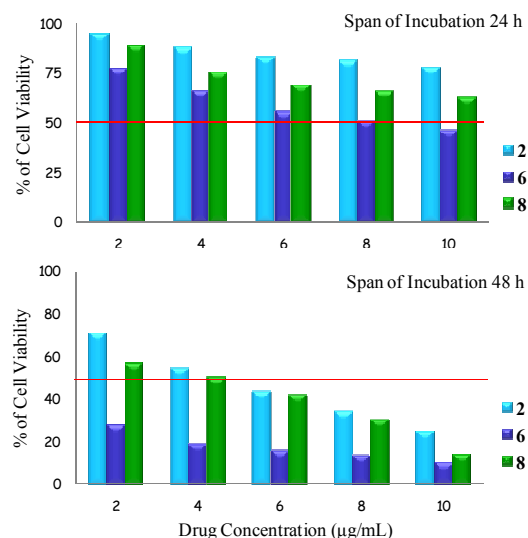


**Fig. 10** Potency of complexes **2**, **6** and **8** on HepG2 cells, after 24 h (a) and 48 h (b) incubation. All determinations are expressed as a percentage of control (untreated cells).

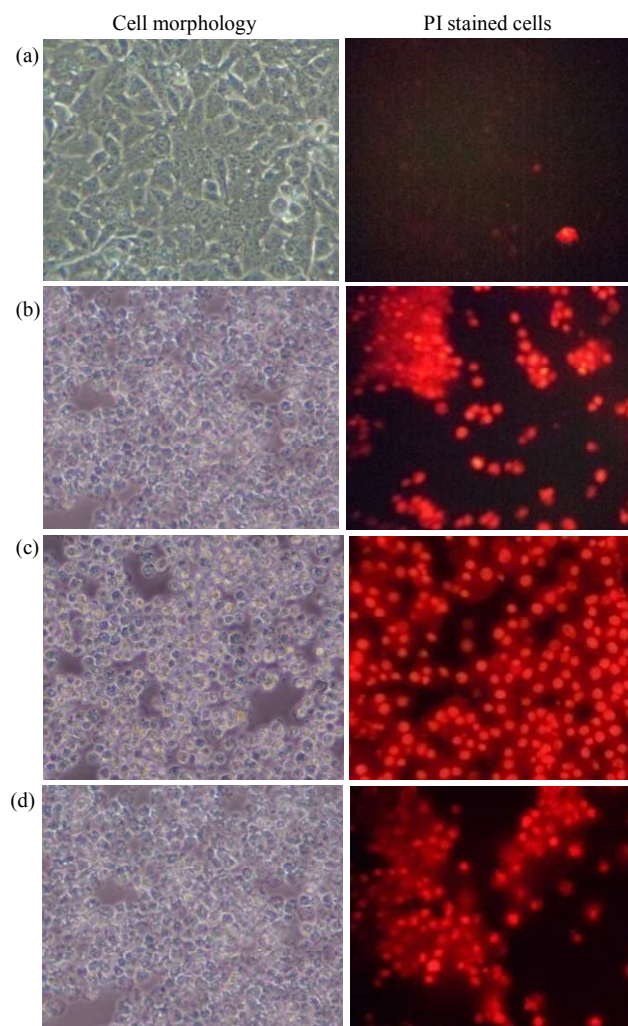


**Fig. 11** Morphological and propidium iodide fluorescent staining of HepG2 cells. Untreated cells (a), treatment of **2** (b), **6** (c) and **8** (d) with the IC<sub>50</sub> concentration (20X Magnification).

The observed IC<sub>50</sub> values reveal that the copper(II) complex **6** exhibited higher *in vitro* cytotoxicity against selected cancer cell line than **8** and **2**, and also relatively equal to cisplatin. The metal complexes exhibit higher mortality at short time with lower concentration compared to others with higher concentration at longer duration. The bio-activities of anticancer metal complexes are dependent on their ability to bind with DNA and damage its structure resulting in the impairment of its function, which is followed by inhibition of replication and transcription processes and, eventually cell death, if the DNA lesions are not properly repaired.<sup>51</sup> Further, it is also observed that the cytotoxicity of complexes increases with increase in reduction potential or easily oxidizable species.<sup>52</sup> Thus, it is possible to correlate the cytotoxicity with redox potential. From CV data it is clear that the oxidizing tendency of complexes lies in the order corresponding with its ligands, L<sup>2</sup> > L<sup>4</sup> based on the substituent at the *para* position and the cytotoxicity follows the same order of an oxidizing tendency of complexes.

**Cell morphology observation:** Radical light inverted microscope was used to monitor the microscopic observations (**Fig. 11**), wherein treated cells showed obvious cellular morphological changes indicating unhealthy cells, whereas the control appeared normal. Control cells were irregular confluent aggregates with rounded and polygonal cells. The cells treated by complexes **2**, **6** and **8** appeared to shrink, became spherical shape and cell spreading patterns were restricted.

**Propidium iodide staining:** Two types of cell death can be observed: An accidental cell death (necrosis) and programmed cell death (apoptosis). In necrosis, the cells undergo cell lysis and lose their membrane integrity, and severe inflammation is induced. However, apoptotic cells are transformed into small membrane-bound vesicles (apoptotic bodies) which are engulfed *in vivo* by macrophages, and no inflammatory response is found. Harmless removal of cells (cancer cells, for example) is one consideration in chemotherapy. Therefore, induction of apoptosis is one of the considerations in the development of anticancer drugs.

Apoptosis is a naturally occurring gene-controlled process that plays a major role in tissue homeostasis and elimination of unwanted cells in animals without affecting normal/unaffected cells. Most of the cancer cells still remain sensitive to some apoptotic stimuli from chemo therapeutic agents, and in this context, the apoptosis-inducing ability of drugs seems to be a primary factor in determining their efficacy.<sup>53</sup> Therefore, we have studied the mode of cell death induced by complexes **2**, **6** and **8** by adopting fluorescent staining for morphological assessment of cell death, single-cell gel electrophoresis (Comet assay) for detecting DNA fragmentation of the treated cells against control cells. Fluorescent dye PI is used to differentiate necrotic, apoptotic and normal cells of HepG2 cell line after treatment with the complexes.

**Fig. 11** shows the characteristic morphological changes brought about in the cells by treatment with complexes **2**, **6** and **8**. The results obtained indicate that complexes induce cell death through different modes like mitotic catastrophe, necrosis and apoptosis. After treating the cells with IC<sub>50</sub> concentration of complexes at different time intervals (24 and 48 h), we have observed cytological changes such as chromatin fragmentation, bi- and multinucleation, cytoplasmic vacuolation, nuclear

swelling, cytoplasmic blebbing, and late apoptosis indication of dot-like chromatin condensation by adopting PI staining. PI staining of cell nuclei has significantly reduced the microscope time required for counting and for evaluating gross cell morphology.

The dead cells are viewed as red colour after staining with PI under the fluorescent light. A very negligible number of PI positive cells were observed in the control and more number of PI positive cells was observed in the case of cancer cells treated with complexes. The observed morphological changes suggest that complexes **6** and **8** possesses higher efficacy than **2** in killing the cells by apoptosis. The mechanism of cell death induced by complexes on liver carcinoma cell line (HepG2) appears to be apoptosis, as evidenced by fluorescent PI staining.

**Alkaline single-cell gel electrophoresis analysis:** The single-cell gel electrophoresis assay (Comet assay) is considered as a rapid, simple, non-invasive, sensitive, visual and inexpensive technique to assess DNA fragmentation typical of toxic DNA damage and of an early stage of apoptosis,<sup>54</sup> as compared to other techniques used for measuring and analyzing DNA strand breaks in mammalian cells. Comet assay gives an image of the changes that have occurred in the chromatin organization in a single-cell which is considered more accurate way to detect early nuclear changes in a cell population. DNA fragmentation is one of the characteristic features observed in apoptotic cells and is generally considered as the biochemical hallmark of the apoptosis, mitotic catastrophe or both and is detected at a single-cell level by the use of single-cell gel electrophoresis in agarose gel matrix. When a cell with damaged DNA is subjected to electrophoresis and then stained with EtBr, it appears as a comet, and the length of the comet tail represents the extent of DNA damage.<sup>55</sup> Comets form as the broken ends of the negatively charged DNA molecules becomes free to migrate in the electric field toward the anode. Major understand about comet formation based on: (i) DNA migration is a function of both size and the number of broken ends of the DNA, and (ii) tail length increases with damage initially and then reaches a maximum. The comet tail length was analyzed by CASP software (**Fig. S12**).

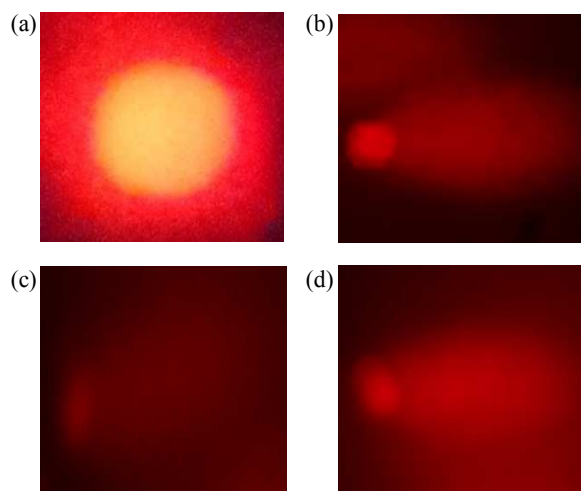


**Fig. 12** Analysis of apoptotic inducing effect of control (a) and complexes **2** (b), **6** (c) and **8** (d) on HepG2 cells assessed by comet assay.

Cells treated with complexes shows statistically significant well-formed comets, whereas the control (untreated) cells fail to show a comet or broom-like tail appearance. The typical photos of the nucleoids of control cells were uniformly spherical in shape, reflecting the absence of any DNA damage. However, upon complete scoring of the nucleoids in experiments, reflecting a baseline level of DNA single-strand breaks. Hence, the average comet score of tail DNA for control HepG2 cells was 2.7% (Fig. 12). In contrast, comet score for complexes show significant numbers of nucleoids with larger comet tails, indicative of higher levels of DNA single-strand breaks. The comet assay score (%) of tail DNA for complexes **2**, **6** and **8** were 64.99, 82.12 and 73.38, respectively. These results implies that complexes significantly increased number of tail DNA, tail length, tail moment and olive tail moment in HepG2 cell line when compared to control cells. The percentage of cells with tail DNA increased significantly after the cells were treated with complexes **2**, **6** and **8** (Table 2). Also, for 24 h treatment the tail length observed for **6** is longer than others, which is consistent with the higher cytotoxicity and the morphological changes observed inside the cell. This clearly indicates that **6** indeed induce DNA fragmentation, which is further evidence for its higher ability to induce apoptotic cell death. On the basis of DNA fragmentation, the potency of the dinuclear complexes in anticancer activity follows the order  $6 > 8 > 2$ .

Results shows the higher anticancer potency of the copper(II) complexes, which are comparable with the widely used drug cisplatin against HepG2 cell line. The present chloro-bridged phenolic complexes exhibit the moderate anticancer activity when compared to the reported phenolic complexes against the same cell line.<sup>56</sup> The outcome of the comet assay shows that a single cell's DNA underwent degradation as consequence of direct DNA damage or rapid apoptosis. The high level of DNA damage induced by complexes reinforces the above results obtained by MTT and fluorescent staining assays. The results of MTT assay, the morphological assessment of cell death and comet assay revealed that complex **6** possesses a very prominent cytotoxicity than others, which is consistent with its strong DNA binding involving hydrophobic forces of interaction and efficient DNA cleavage and potent radical scavenging property.

## Conclusions

In summary, a new series of chloro-bridged nickel(II) and copper(II) complexes **1–8** were synthesized and characterized. Single crystal X-ray investigation of complexes  $[(\text{NiL}^4(\text{CH}_3\text{OH})_2)_2(\mu\text{-Cl})](\text{Cl})_3 \cdot (\text{H}_2\text{O})_2$ , (**4**) and  $[(\text{CuL}^4\text{Cl})_2(\mu\text{-Cl})\text{Cl} \cdot (\text{H}_2\text{O})_7]$ , (**8**) revealed distorted octahedral and square-pyramidal geometry, respectively, around the metal ions. Thermodynamic stability constants and thermodynamic parameters of the complexes have been determined spectrophotometrically. The temperature dependent magnetic susceptibility measurements of the copper(II) complexes (**5–8**) indicate strong antiferromagnetic coupling exchange interaction between the adjacent copper ions. The antioxidant property implies that complex **6** possesses effective radical scavenging activity against DPPH in terms of  $\text{IC}_{50}$  values. The DNA binding studies implies the partial intercalation along with electrostatic mode of binding with CT-DNA. The complex **6** displayed higher DNA binding propensity

and nuclease activity than the other dinuclear complexes. Mechanistic studies of the nuclease activity indicated the possible role of hydroxyl radical as reactive oxygen species. Assay results suggest that, complexes **2**, **6** and **8** exhibit apoptotic cell death against HepG2 cancer cells. Remarkably, complex **6** exhibit the highest anticancer activity with an  $\text{IC}_{50}$  value of 9.5  $\mu\text{M}$ , relatively equal to the widely used drug cisplatin ( $\text{IC}_{50}$ , 10.5  $\mu\text{M}$ ) against the same cell line. Apoptotic cell death was further evidenced from alkaline single-cell gel electrophoresis, and the assay results show that complexes indeed induce DNA fragmentation. This implies that a synergic combination of ligand and metal ion is important in the design of a potential anticancer drug, which correlates well with the ability of complexes to strongly bind and cleave DNA. The results obtained from the present work would be helpful to design and develop new chloro-bridged dinuclear complexes as potent therapeutic and anticancer agents for some chronic diseases.

## Experimental

### General methods and materials

Micro analysis (% CHN) was performed using Carlo Erba model 1106 elemental analyzer. IR spectra of ligands and complexes were recorded using KBr pellets in the range 4000–400  $\text{cm}^{-1}$  on a Bruker Alpha FT-IR spectrophotometer. The  $^1\text{H}$  NMR spectra of the nickel(II) complexes were collected on VNMRS-400 spectrometer in DMSO ( $d_6$ ) at room temperature. UV-Vis spectra of complexes were recorded in HPLC grade DMF at 25 °C on Agilent-8453 spectrophotometer in the range of 200–1100 nm. ESI mass spectra were recorded on a Q-ToF micromass spectrograph using  $\text{H}_2\text{O}$  as the mobile phase with an approximate concentration of 1.0  $\text{mmol dm}^{-3}$ . Cyclic voltammograms were obtained on CHI 602D (CH Instruments Co., USA) electrochemical analyzer under oxygen free conditions using a three-electrode cell with a DMF solution of TBAP (0.1 M) as the supporting electrolyte. A Pt wire, glassy carbon, and the Ag/AgCl electrode (saturated KCl solution) were used as counter, working and reference electrode, respectively. A Ferrocene/ferrocenium ( $\text{Fc}/\text{Fc}^+$ ) couple was used as an internal standard. The reported potentials are relative to the Ag/AgCl electrode and  $E_{1/2}$  of the  $\text{Fc}/\text{Fc}^+$  couple. The concentration of complex solutions were taken around  $1.0 \times 10^{-3}$  M and, the scan rate was 100  $\text{mVs}^{-1}$ . Molar conductivity was measured with an Elico digital conductivity bridge model CM-88, using a freshly prepared DMF solution of complex. X-band EPR spectra of the Cu(II) complexes were recorded at room temperature on a Varian EPR-E 112 spectrometer. The magnetic measurements were carried out on a PAR vibrating sample magnetometer (Model-155). The  $\chi_{\text{MT}}$  data were collected over the temperature range 20–300 K with an applied magnetic field of 5000 Oe and instrument was calibrated using metallic nickel.

The ligands 2-((2-(piperazin-1-yl)ethylimino)methyl)phenol ( $\text{L}^1$ ), 4-methyl-2-((2-(piperazin-1-yl)ethylimino)methyl)phenol ( $\text{L}^2$ ), 4-chloro-2-((2-(piperazin-1-yl)ethylimino)methyl)phenol ( $\text{L}^3$ ) and 4-bromo-2-((2-(piperazin-1-yl)ethylimino)methyl)phenol ( $\text{L}^4$ ) were prepared by condensation of 1-(2-aminoethyl) piperazine with corresponding salicylaldehyde in methanol.<sup>13</sup> All reagents and chemicals were purchased from commercial sources (SRL and S.D. Fine chemicals, India; Sigma-Aldrich, USA) and used without further purification. Solvents were dried and purified

before being used according to standard procedure. Tetra(*n*-butyl) ammonium perchlorate (TBAP) used as the supporting electrolyte in the electrochemical measurements, was purchased from Fluka (Switzerland) and recrystallized from hot methanol. The calf thymus (CT) and pBR322 DNA were purchased from Bangalore Genei (India). Ethidium bromide (EtBr) was obtained from Sigma-Aldrich (USA).

### Synthesis of dinuclear complexes

The chloro-bridged dinuclear nickel(II) **1–4** and copper(II) **5–8** complexes were prepared by following general synthetic procedure. To a stirred methanolic solution (10 mL) of NiCl<sub>2</sub>·6H<sub>2</sub>O (0.232 g, 1 mmol) or CuCl<sub>2</sub>·2H<sub>2</sub>O (0.170 g, 1 mmol), a methanolic solution (10 mL) of appropriate ligand L<sup>1–4</sup> (1 mmol) was added slowly and stirring was continued for 2 h. The reaction mixture was refluxed for 6 h, filtered hot and kept aside for slow evaporation. The product was washed with cold methanol and dried *in vacuo*.

**[(NiL<sup>1</sup>(CH<sub>3</sub>OH)<sub>2</sub>)<sub>2</sub>(μ-Cl)](Cl)<sub>3</sub>·(H<sub>2</sub>O)<sub>2</sub> (**1**):** Yield: 0.76 g (85.4%). Colour: Green. Anal. Calc. for C<sub>30</sub>H<sub>58</sub>Cl<sub>4</sub>N<sub>6</sub>Ni<sub>2</sub>O<sub>8</sub>, (FW: 890.01): C, 40.48; H, 6.57; N, 9.44%. Found: C, 40.45; H, 6.61; N, 9.42%. Selected IR data (KBr, ν, cm<sup>-1</sup>): 3388 ν(O–H str. of CH<sub>3</sub>OH), 2947 ν(N–H str. of >NH<sub>2</sub><sup>+</sup>), 1650 ν(C=N), 1549 ν(N–H bend. of >NH<sub>2</sub><sup>+</sup>), 1292 ν(Ar–O). UV-Vis (DMF), λ/nm (ε/M<sup>-1</sup> cm<sup>-1</sup>): 268 (19,184), 372 (11,465), 634 (938), 930 (315) nm. ESI-MS (H<sub>2</sub>O) display peaks at: [NiL<sup>1</sup> + H]<sup>2+</sup> (292), [NiL<sup>1</sup>]<sup>+</sup> (291). Conductance (A<sub>M</sub>, Ω<sup>-1</sup> cm<sup>2</sup> mol<sup>-1</sup>) in DMF: 291.

**[(NiL<sup>2</sup>(CH<sub>3</sub>OH)<sub>2</sub>)<sub>2</sub>(μ-Cl)](Cl)<sub>3</sub>·(H<sub>2</sub>O)<sub>2</sub> (**2**):** Yield: 0.79 g (86%). Colour: Pale Green. Anal. Calc. for C<sub>32</sub>H<sub>62</sub>Cl<sub>4</sub>N<sub>6</sub>Ni<sub>2</sub>O<sub>8</sub>, (FW: 918.07): C, 41.86; H, 6.81; N, 9.15%. Found: C, 41.83; H, 6.86; N, 9.12%. Selected IR data (KBr, ν, cm<sup>-1</sup>): 3406 ν(O–H str. of CH<sub>3</sub>OH), 2964 ν(N–H str. of >NH<sub>2</sub><sup>+</sup>), 1649 ν(C=N), 1546 ν(N–H bend. of >NH<sub>2</sub><sup>+</sup>), 1290 ν(Ar–O). UV-Vis (DMF), λ/nm (ε/M<sup>-1</sup> cm<sup>-1</sup>): 268 (19,485), 381 (13,905), 644 (1,830), 930 (894) nm. ESI-MS (H<sub>2</sub>O) display peaks at: [NiL<sup>2</sup> + H]<sup>2+</sup> (307), [NiL<sup>2</sup>]<sup>+</sup> (305). Conductance (A<sub>M</sub>, Ω<sup>-1</sup> cm<sup>2</sup> mol<sup>-1</sup>) in DMF: 294.

**[(NiL<sup>3</sup>(CH<sub>3</sub>OH)<sub>2</sub>)<sub>2</sub>(μ-Cl)](Cl)<sub>3</sub>·(H<sub>2</sub>O)<sub>2</sub> (**3**):** Yield: 0.78 g (81.3%). Colour: Green. Anal. Calc. for C<sub>30</sub>H<sub>56</sub>Cl<sub>6</sub>N<sub>6</sub>Ni<sub>2</sub>O<sub>8</sub>, (FW: 958.90): C, 37.58; H, 5.89; N, 8.76%. Found: C, 37.55; H, 5.93; N, 8.77%. Selected IR data (KBr, ν, cm<sup>-1</sup>): 3384 ν(O–H str. of CH<sub>3</sub>OH), 2957 ν(N–H str. of >NH<sub>2</sub><sup>+</sup>), 1655 ν(C=N), 1536 ν(N–H bend. of >NH<sub>2</sub><sup>+</sup>), 1294 ν(Ar–O). UV-Vis (DMF), λ/nm (ε/M<sup>-1</sup> cm<sup>-1</sup>): 268 (15,898), 382 (10,392), 624 (1,637), 954 (765) nm. ESI-MS (H<sub>2</sub>O) display peaks at: [NiL<sup>3</sup> + H]<sup>2+</sup> (326), [NiL<sup>3</sup>]<sup>+</sup> (325). Conductance (A<sub>M</sub>, Ω<sup>-1</sup> cm<sup>2</sup> mol<sup>-1</sup>) in DMF: 282.

**[(NiL<sup>4</sup>(CH<sub>3</sub>OH)<sub>2</sub>)<sub>2</sub>(μ-Cl)](Cl)<sub>3</sub>·(H<sub>2</sub>O)<sub>2</sub> (**4**):** Yield: 0.73 g (69.7%). Colour: Dark green. Anal. Calc. for C<sub>30</sub>H<sub>56</sub>Br<sub>2</sub>Cl<sub>4</sub>N<sub>6</sub>Ni<sub>2</sub>O<sub>8</sub>, (FW: 1047.81): C, 34.39; H, 5.39; N, 8.02%. Found: C, 34.37; H, 5.42; N, 8.05%. Selected IR data (KBr, ν, cm<sup>-1</sup>): 3379 ν(O–H str. of CH<sub>3</sub>OH), 2952 ν(N–H str. of >NH<sub>2</sub><sup>+</sup>), 1637 ν(C=N), 1524 ν(N–H bend. of >NH<sub>2</sub><sup>+</sup>), 1309 ν(Ar–O). UV-Vis (DMF), λ/nm (ε/M<sup>-1</sup> cm<sup>-1</sup>): 268 (17,099), 369 (10,826), 630 (1,039), 973 (638) nm. ESI-MS (H<sub>2</sub>O) display peaks at: [NiL<sup>4</sup> + H]<sup>2+</sup> (371), [NiL<sup>4</sup>]<sup>+</sup> (370). Conductance (A<sub>M</sub>, Ω<sup>-1</sup> cm<sup>2</sup> mol<sup>-1</sup>) in DMF: 285.

**[(CuL<sup>1</sup>Cl)<sub>2</sub>(μ-Cl)]Cl·(H<sub>2</sub>O)<sub>7</sub> (**5**):** Yield: 0.63 g (73.1%). Colour: Green. Anal. Calc. for C<sub>26</sub>H<sub>52</sub>Cl<sub>4</sub>N<sub>6</sub>Cu<sub>2</sub>O<sub>9</sub>, (FW: 861.63): C,

36.24; H, 6.08; N, 9.75%. Found: C, 36.22; H, 6.14; N, 9.73%. Selected IR data (KBr, ν, cm<sup>-1</sup>): 3423 ν(O–H str. of H<sub>2</sub>O), 2955 ν(N–H str. of >NH<sub>2</sub><sup>+</sup>), 1643 ν(C=N), 1544 ν(N–H bend. of >NH<sub>2</sub><sup>+</sup>), 1296 ν(Ar–O). UV-Vis (DMF), λ/nm (ε/M<sup>-1</sup> cm<sup>-1</sup>): 272 (16,285), 359 (6,422), 657 (278) nm. ESI-MS (H<sub>2</sub>O) display peaks at: [CuL<sup>1</sup> + 2H]<sup>2+</sup> (298), [CuL<sup>1</sup>]<sup>+</sup> (296). Conductance (A<sub>M</sub>, Ω<sup>-1</sup> cm<sup>2</sup> mol<sup>-1</sup>) in DMF: 131. g<sub>||</sub> = 2.16. μ<sub>eff</sub> = 1.51 BM, -2J = 236 cm<sup>-1</sup> at 298 K.

**[(CuL<sup>2</sup>Cl)<sub>2</sub>(μ-Cl)]Cl·(H<sub>2</sub>O)<sub>7</sub> (**6**):** Yield: 0.64 g (77.6%). Colour: Green. Anal. Calc. for C<sub>28</sub>H<sub>56</sub>Cl<sub>4</sub>N<sub>6</sub>Cu<sub>2</sub>O<sub>9</sub>, (FW: 889.68): C, 37.80; H, 6.34; N, 9.45%. Found: C, 37.81; H, 6.38; N, 9.43%. Selected IR data (KBr, ν, cm<sup>-1</sup>): 3452 ν(O–H str. of H<sub>2</sub>O), 2934 ν(N–H str. of >NH<sub>2</sub><sup>+</sup>), 1642 ν(C=N), 1538 ν(N–H bend. of >NH<sub>2</sub><sup>+</sup>), 1303 ν(Ar–O). UV-Vis (DMF), λ/nm (ε/M<sup>-1</sup> cm<sup>-1</sup>): 274 (14,302), 358 (5,428), 668 (221) nm. ESI-MS (H<sub>2</sub>O) display peaks at: [CuL<sup>2</sup> + 2H]<sup>2+</sup> (311), [CuL<sup>2</sup>]<sup>+</sup> (309). Conductance (A<sub>M</sub>, Ω<sup>-1</sup> cm<sup>2</sup> mol<sup>-1</sup>) in DMF: 137. g<sub>||</sub> = 2.15. μ<sub>eff</sub> = 1.52 BM, -2J = 239 cm<sup>-1</sup> at 298 K.

**[(CuL<sup>3</sup>Cl)<sub>2</sub>(μ-Cl)]Cl·(H<sub>2</sub>O)<sub>7</sub> (**7**):** Yield: 0.71 g (76.3%). Colour: Dark green. Anal. Calc. for C<sub>26</sub>H<sub>50</sub>Cl<sub>6</sub>N<sub>6</sub>Cu<sub>2</sub>O<sub>9</sub>, (FW: 930.52): C, 33.56; H, 5.42; N, 9.03%. Found: C, 33.54; H, 5.47; N, 9.01%. Selected IR data (KBr, ν, cm<sup>-1</sup>): 3442 ν(O–H str. of H<sub>2</sub>O), 2949 ν(N–H str. of >NH<sub>2</sub><sup>+</sup>), 1646 ν(C=N), 1549 ν(N–H bend. of >NH<sub>2</sub><sup>+</sup>), 1304 ν(Ar–O). UV-Vis (DMF), λ/nm (ε/M<sup>-1</sup> cm<sup>-1</sup>): 272 (21,815), 358 (9,934), 658 (423) nm. ESI-MS (H<sub>2</sub>O) display peaks at: [CuL<sup>3</sup> + 2H]<sup>2+</sup> (332), [CuL<sup>3</sup>]<sup>+</sup> (330). Conductance (A<sub>M</sub>, Ω<sup>-1</sup> cm<sup>2</sup> mol<sup>-1</sup>) in DMF: 125. g<sub>||</sub> = 2.19. μ<sub>eff</sub> = 1.49 BM, -2J = 220 cm<sup>-1</sup> at 298 K.

**[(CuL<sup>4</sup>Cl)<sub>2</sub>(μ-Cl)]Cl·(H<sub>2</sub>O)<sub>7</sub> (**8**):** Yield: 0.76 g (74.5%). Colour: Dark green. Anal. Calc. for C<sub>26</sub>H<sub>50</sub>Br<sub>2</sub>Cl<sub>4</sub>N<sub>6</sub>Cu<sub>2</sub>O<sub>9</sub>, (FW: 1019.42): C, 30.63; H, 4.94; N, 8.24%. Found: C, 30.61; H, 4.99; N, 8.21%. Selected IR data (KBr, ν, cm<sup>-1</sup>): 3419 ν(O–H str. of H<sub>2</sub>O), 2929 ν(N–H str. of >NH<sub>2</sub><sup>+</sup>), 1647 ν(C=N), 1526 ν(N–H bend. of >NH<sub>2</sub><sup>+</sup>), 1304 ν(Ar–O). UV-Vis (DMF), λ/nm (ε/M<sup>-1</sup> cm<sup>-1</sup>): 269 (14,125), 372 (5,734), 655 (262) nm. ESI-MS (H<sub>2</sub>O) display peaks at: [CuL<sup>4</sup> + 2H]<sup>2+</sup> (362), [CuL<sup>4</sup>]<sup>+</sup> (360). Conductance (A<sub>M</sub>, Ω<sup>-1</sup> cm<sup>2</sup> mol<sup>-1</sup>) in DMF: 128. g<sub>||</sub> = 2.18. μ<sub>eff</sub> = 1.50 BM, -2J = 228 cm<sup>-1</sup> at 298 K.

### Single crystal X-ray diffraction

Single crystals of complexes **4** and **8** suitable for XRD measurements were sorted using polarizing microscope (Leica DMLSP). Crystals having good morphology were chosen for three-dimensional intensity data collection. Crystals with three dimensions of 0.30 × 0.25 × 0.20 and 0.30 × 0.20 × 0.20 mm for complexes **4** and **8**, respectively were mounted on a glass fiber for diffraction experiment. X-ray single crystal data were collected on a Kappa Apex2 CCD diffractometer equipped with a fine-focus sealed tube X-ray source and graphite monochromated Mo (Kα) radiation in the wavelength (λ) of 0.71073 Å at room temperature (293 ± 2 K). The intensity data were collected using ω and φ scans with frame width of 0.5°. The frame integration and data reduction were performed using Bruker SAINT-plus (Version 7.06a) software. Empirical absorption corrections were applied for complexes, using SADABS program.<sup>57</sup> The structure was solved by using SIR92<sup>58</sup> and the full-matrix least-squares refinement on F<sup>2</sup> was performed using SHELXL-97 program.<sup>59</sup>

**Table 4** Crystal data and structure refinement for complexes **4** and **8**

Complex	4	8
CCDC	907779	952060
Empirical Formula	C <sub>30</sub> H <sub>56</sub> Br <sub>2</sub> Cl <sub>4</sub> N <sub>6</sub> Ni <sub>2</sub> O <sub>8</sub>	C <sub>26</sub> H <sub>50</sub> Br <sub>2</sub> Cl <sub>4</sub> N <sub>6</sub> Cu <sub>2</sub> O <sub>9</sub>
Formula Weight	1047.85	1019.42
Temperature (K)	293 ± 2	293 ± 2
Wavelength (Å)	0.71073	0.71073
Crystal system	Monoclinic	Monoclinic
Space group	C2/c	P21/n
<i>a</i> (Å)	10.1699(4)	13.8391(4)
<i>b</i> (Å)	16.8523(8)	14.3968(4)
<i>c</i> (Å)	24.8924(11)	20.2234(7)
$\alpha$ (°)	90	90
$\beta$ (°)	98.768(2)	98.6740(10)
$\gamma$ (°)	90	90
Volume (Å <sup>3</sup> )	4216.4(3)	3983.2(2)
<i>Z</i>	4	4
Calculated density (Mg/m <sup>3</sup> )	1.651	1.700
Absorption coefficient (mm <sup>-1</sup> )	3.094	3.395
<i>F</i> (000)	2144	2064
Crystal size (mm)	0.30 × 0.25 × 0.20	0.30 × 0.20 × 0.20
$\theta$ range for data collection (°)	2.36–28.81	2.05–26.98
Limiting indices	–13 ≤ <i>h</i> ≤ 13, –22 ≤ <i>k</i> ≤ 22, –33 ≤ <i>l</i> ≤ 33	–17 ≤ <i>h</i> ≤ 17, –18 ≤ <i>k</i> ≤ 18, –25 ≤ <i>l</i> ≤ 25
Reflections collected	23444	41141
Independent reflections	5502 [ <i>R</i> (int) = 0.0339]	8638 [ <i>R</i> (int) = 0.0667]
Max. and min. transmission	0.5766 and 0.4571	0.592 and 0.501
Refinement method	Full-matrix least-squares on <i>F</i> <sup>2</sup>	Full-matrix least-squares on <i>F</i> <sup>2</sup>
Data/restraints/parameters	5502/74/305	8638/6/456
GOF on <i>F</i> <sup>2</sup>	1.037	1.055
Final <i>R</i> indices [ <i>I</i> > 2σ( <i>I</i> )]	<i>R</i> 1 = 0.0333, <i>wR</i> 2 = 0.0740	<i>R</i> 1 = 0.0426, <i>wR</i> 2 = 0.0923
<i>R</i> indices (all data)	<i>R</i> 1 = 0.0574, <i>wR</i> 2 = 0.0816	<i>R</i> 1 = 0.0894, <i>wR</i> 2 = 0.1107
Largest diff. peak and hole (e.Å <sup>-3</sup> )	0.581 and –0.5000	0.716 and –0.617

The scattering factors incorporated in SHELXL-97 were used. After several cycles of refinement, the positions of hydrogen atoms were calculated and added to the refinement process. Molecular graphics, hydrogen bonding and packing figures were generated by using the softwares ORTEP 3.0<sup>60</sup> and Mercury 3.0.<sup>61</sup> Details of the crystallographic data and structure refinement parameters for complexes **4** and **8** are summarized in **Table 4**.

CCDC 907779 (for **4**) and 952060 (for **8**). For crystallographic data in CIF or other electronic format see DOI: 10.1039/b000000x/.

#### 10 DPPH radical scavenging activity

An electron (or) hydrogen atom donation (or) free radical scavenging abilities of complexes was evaluated from the bleaching of DPPH in methanolic medium. A 0.1 mM DPPH solution was used to generate the stable radical<sup>62</sup> and, the absorbance was measured for this DPPH solution at 517 nm (*A*<sub>blank</sub>). Complexes of different concentrations (0–250 μM) were prepared in DMF and added (1 mL) to each DPPH solutions. The reaction mixtures were incubated for 30 min at room temperature (in dark) and the absorbance of these solutions (*A*<sub>sample</sub>) was measured at 517 nm against blank. DPPH free radical scavenging activity (or) inhibition (I%) of DPPH radicals for the various concentration of complexes were calculated from the following expression,

$$I\% = (A_{\text{blank}} - A_{\text{sample}}/A_{\text{blank}}) \times 100$$

The IC<sub>50</sub> values were calculated by plotting I% values as a function of complex concentrations.

#### DNA binding studies

**Absorption spectral titration:** The application of electronic absorption spectra in DNA interaction is one of the most effective method to examine the binding mode and strength of metal complexes with DNA. A solution of calf thymus DNA in Tris-HCl buffer (5 mM Tris-HCl/50 mM NaCl, pH = 7.2) gave a ratio of UV absorbance at 260 and 280 nm (*A*<sub>260</sub>/*A*<sub>280</sub>) of about 1.87:1, indicating that the DNA was sufficiently free from proteins.<sup>63</sup> Stock solutions of CT-DNA was prepared in Tris-HCl/NaCl buffer and stored at 4 °C for less than 4 days. The DNA concentration per nucleotide was determined from the absorption intensity at 260 nm using the molar absorption coefficient of 6600 M<sup>-1</sup> cm<sup>-1</sup>.<sup>64</sup> Stock solutions of complexes was prepared by using 5% DMF/Tris-HCl (0.5 mL DMF in 10 mL buffer) and diluting suitably with the corresponding buffer to the required concentrations for all the experiments. Absorption titration experiments were carried out by varying nucleic acid concentration (0–500 μM) and maintaining complex concentration constant (50 μM). Complex-DNA solutions were allowed to incubate for 30 min at room temperature before measurements were taken. While measuring the absorption spectra, equal amounts of DNA was added to both complex solution and the reference solution to eliminate the absorbance of DNA itself. Absorbances were recorded after each successive addition of DNA solution at room temperature. Titration curves were constructed from the fractional change in the absorption

intensity as a function of DNA concentration.<sup>40</sup> The intrinsic binding constant  $K_b$  can be obtained by the following equation:

$$[\text{DNA}]/(\varepsilon_a - \varepsilon_f) = [\text{DNA}]/(\varepsilon_b - \varepsilon_f) + 1/K_b(\varepsilon_b - \varepsilon_f)$$

where, [DNA] is the DNA concentration in M (nucleotide),  $\varepsilon_a$  – apparent extinction coefficient obtained by calculating  $A_{\text{observed}}/[\text{Complex}]$ ,  $\varepsilon_f$  – extinction coefficient of complex in its free form,  $\varepsilon_b$  – extinction coefficient of complex in the fully bound form.  $K_b$  – is the intrinsic binding constant in  $\text{M}^{-1}$ . Each set of data were fitted to the above equation, and the plot of [DNA]/ $(\varepsilon_a - \varepsilon_f)$  versus [DNA] gave a slope and the  $y$ -intercept which are equal to  $1/(\varepsilon_b - \varepsilon_f)$  and  $1/K_b(\varepsilon_b - \varepsilon_f)$ , respectively. The intrinsic binding constant  $K_b$  was obtained from the ratio of the slope to the intercept.

**Hydrodynamic (Viscosity) measurements:** Viscometric experiments were conducted on an Ostwald micro viscometer of 2 mL capacity, immersed in a water bath maintained at  $25 \pm 0.1$  °C. The solutions of DNA (200  $\mu\text{M}$ ) and complexes (0–100  $\mu\text{M}$ ) were prepared by using Tris-HCl/NaCl buffer (pH = 7.2). Mixing of the solution was achieved by purging nitrogen gas through viscometer. The flow time was measured with a digital stopwatch and the experiment was repeated in triplicate to get the concurrent values. Data were presented as  $(\eta/\eta_0)^{1/3}$  versus binding ratio (1/R) [Complex] / [DNA],<sup>65</sup> where  $\eta$  and  $\eta_0$  are the specific viscosity of DNA in the presence and absence of complex, respectively. The values of  $\eta$  and  $\eta_0$  were calculated from the relation,<sup>41</sup>

$$\eta = (t - t_b)/t_b$$

where,  $t_b$  is the flow time of buffer alone and,  $t$  is the observed flow time for DNA in the absence and presence of complex. Relative viscosities for DNA were obtained from the relation,  $\eta/\eta_0$ .

**Electrochemical titration:** Electrochemical techniques are best complementary to other related biophysical techniques that are applied to study the interaction between redox active molecules and bio-molecules.<sup>66</sup> The solutions of complexes and DNA were prepared by using DMF and Tris-HCl/NaCl buffer (pH 7.2), respectively, in double distilled water. The concentration of complexes can be taken as 100  $\mu\text{M}$  and also for DNA. Solutions were deaerated by purging with  $\text{N}_2$  gas for 5 minutes prior to the measurements.

#### 40 Nuclease activity

The nuclease activity of complexes 1–8 on supercoiled plasmid DNA (pBR322) was monitored using agarose gel electrophoresis technique by determining its ability to convert supercoiled DNA (Form I) to nicked circular (Form II) and linear forms (Form III). In the cleavage reactions, plasmid DNA (33.3  $\mu\text{M}$ ) was treated with complexes (0–250  $\mu\text{M}$ ) and hydrogen peroxide (0.1 mM, co-reactant) in Tris-HCl/NaCl buffer (pH 7.2). To test the involvement of reactive oxygen species (ROS) during strand scission, we further investigated the influence of the hydroxyl radical scavenger (DMSO, 10 mM) during the cleavage reaction. The mixture was incubated for 1 h at 37 °C. A loading buffer containing 0.25% bromophenol blue, 0.25% xylene cyanol, 30% glycerol (3  $\mu\text{L}$ ) was added and the electrophoresis of cleavage products were performed on 0.8% agarose gel containing

ethidium bromide (1  $\mu\text{g}/\text{mL}$ ). The gels were run at 50 V for 1 h in TAE buffer (40 mM Tris base, 20 mM acetic acid, 1 mM EDTA, pH 8.3). The bands were viewed and imaged.

Ligation enzymatic assay was performed using T4 DNA ligase to determine whether the cleaved products consistent with hydrolytic cleavage of DNA. The cleavage product was purified by DNA gel extraction kit and incubated for 12 h at 16 °C with 1.5  $\mu\text{L}$  of 10X ligation buffer, 1  $\mu\text{L}$  of T4 ligase (4 units) and 2.5  $\mu\text{L}$  of 1 mM ATP. Afterwards, the ligation products were stained with EtBr, electrophoresed and imaged.

#### 65 Growth Inhibition studies

**Cell line and cell culture conditions:** Human hepatocellular liver carcinoma cell line (HepG2) and Vero cell line were obtained from National Centre for Cell Science (NCCS), Pune, India. The cancer cells were cultured in Dulbecco's Modified Eagles Medium (DMEM) (St. Louis, Mo, USA), supplemented with 10% Fetal Bovine Serum (FBS) (Sigma Aldrich, USA), 100  $\mu\text{g}/\text{mL}$  of Streptomycin, 20  $\mu\text{g}/\text{mL}$  of Kanamycin acid sulphate and 7.5% sodium bicarbonate solution (Himedia, Mumbai, India) in 96-well culture plates at 37 °C in a humidified atmosphere of 5%  $\text{CO}_2$  in a  $\text{CO}_2$  incubator (Thermoscientific, Germany). MTT [3-(4,5-dimethylthiazol-2-yl)-2,5-diphenyltetrazolium bromide, a yellow tetrazole] was obtained from Himedia. All experiments were performed using cells from fifteenth passage.

**Cell viability assay (MTT assay):** *In vitro* anticancer potency of complexes 2, 6 and 8 was carried out by using MTT assay as described previously.<sup>67</sup> HepG2 cells were cultured and seeded into 96 well plates approximately as  $1 \times 10^5$  cells in each well. Complexes in the concentration range of 2–10  $\mu\text{g}/\text{mL}$  dissolved in deionized water was added to the wells. After treatment, the plates were incubated for 24–48 h in order to perform cytotoxic analysis using MTT assay. MTT was prepared at a concentration of 5 mg/mL and 10  $\mu\text{L}$  of MTT was added in each well and incubated for 4 h. Purple color farmazone crystals formed were then dissolved in 100  $\mu\text{L}$  of dimethyl sulphoxide (DMSO). These crystals were observed at 570 nm in a multi well ELISA plate reader. Optical density value was subjected to percentage of viability (I%) by using the following formula.

$$\text{I\%} = \frac{\text{Mean OD of untreated cells} - \text{Mean OD of treated cells}}{\text{Mean OD of untreated cells}} \times 100$$

#### Apoptosis evaluation by cell morphology and propidium iodide staining:

To detect apoptosis, cells were judged according to their nuclear morphology and disintegration of their cell membranes, which is indicated by propidium iodide (PI) uptake.<sup>68</sup> HepG2 cells were plated at a density of  $1 \times 10^6$  cells/well into a six-well plate and incubated overnight. At 90% confluence, the cells were treated with complexes 2, 6 and 8 at  $\text{IC}_{50}$  dose, washed with PBS fixed in methanol and acetic acid (3:1 v/v) for 10 min and stained with 50  $\mu\text{g}/\text{mL}$  of PI for 20 mins. Nuclear morphology of apoptotic cells with condensed/fragmented nuclei was examined under an Inverted phase contrast/fluorescent microscope (Radical).

**Alkaline single-cell gel electrophoresis assay (Comet assay):** An alkaline single-cell gel electrophoresis (SCGE) technique<sup>69</sup> is a neutral assay, first introduced by Östling and Johanson in 1984 which has been modified and extensively validated over the 5 years, and is now commonly referred to as the 'comet assay'.<sup>70</sup> DNA damage was quantified by adopting comet assay as previously described.<sup>71</sup> Cells used for the comet assay were sampled from a monolayer during the growing phase, 24 h after seeding. Cells were treated with complexes at IC<sub>50</sub> dose and cells 10 were harvested by a trypsinization process. Normal agarose in PBS (200 µL of 1% solution, pH 7.4) at 65 °C was dropped gently onto a fully frosted micro slide, covered immediately with a cover slip, and then placed over a frozen ice pack for ~5 min. The cover slip was removed after the gel had set. The cell 15 suspension from each samples, was mixed with 1% low-melting agarose (LMA) at 37 °C in a 1:3 ratio. This mixture (100 µL) was quickly applied on top of the gel, coated over the micro slide, and allowed to set as before. A third coating of 100 µL of 1% LMA was given on the gel containing the cell suspension and allowed 20 to set. After solidification of the agarose, the cover slips were removed and the slides were immersed in ice-cold lytic solution (2.5 M NaCl, 100 mM Na-EDTA, 10 mM Tris-base and 0.1% Triton X100, 10% DMSO, pH 10) and placed in a refrigerator at 4 °C. All the above operations were performed under low lighting 25 conditions to avoid DNA damage due to light. The slides, after being removed from the lytic solution were placed horizontally in an electrophoresis tank. The reservoirs were filled with electrophoresis buffer (300 mM NaOH, 1 mM Na-EDTA, pH 13) until the slides were just immersed in it and allowed to stand in 30 the buffer for 20 min (to allow DNA unwinding), after which electrophoresis was carried out at 0.8 V/cm for 15 min. After electrophoresis, the slides were removed, washed thrice in neutralization buffer (0.4 M Tris, pH 7.5), and gently tapped to dry. Nuclear DNA was stained with 20 µL of propidium iodide 35 (50 µg/mL). Photographs were obtained using an Inverted fluorescence microscope at 20X magnification. The DNA contents in the head and tail were quantified by using CASP software.

## Acknowledgements

AKR gratefully thanks UGC, New Delhi, for financial 40 assistance through the Major Research Project grant [F.No.39-797/2010 (SR)]. The authors thank to SAIF, IIT-M and CLRI, Chennai for Single crystal XRD and EPR studies, respectively.

## References

- (a) G. Zuber, J. C. Quada, Jr. and S. M. Hecht, *J. Am. Chem. Soc.*, 1998, **120**, 9368–9369; (b) S. M. Hecht, *J. Nat. Prod.*, 2000, **63**, 158–168.
- (a) A. R. Banerjee, J. A. Jaeger and D. H. Turner, *Biochemistry*, 1993, **32**, 153–163; (b) Y. Jin and J. A. Cowan, *J. Am. Chem. Soc.*, 2005, **127**, 8408–8415.
- G. Giaccone, R. S. Herbst, C. Manegold, G. Scagliotti, R. Rosell, V. Miller, J. S. Ochs and R. B. Natale, *J. Clin. Oncol.*, 2004, **22**, 777–784.
- T. R. Krugh and J. W. Neely, *Biochemistry*, 1973, **12**, 4418–4425.
- (a) S. Ramakrishnan, E. Suresh, A. Riyasdeen, M. A. Akbarsha and M. Palaniandavar, *Dalton Trans.*, 2011, **40**, 3245–3256; (b) Y. -C. Liu, X. -Y. Song, Z. -F. Chen, Y. -Q. Gu, Y. Peng and H. Liang, *Inorg. Chim. Acta*, 2012, **382**, 52–58.
- (a) P. U. Maheswari, S. Roy, H. D. Dulk, S. Barends, G. V. Wezel, B. Kozlevčar, P. Gamez and J. Reedijk, *J. Am. Chem. Soc.*, 2006, **128**, 710–711; (b) C. Marzano, M. Pellai, F. Tisato and C. Santini, *Anti-Cancer Agent. Med. Chem.*, 2009, **9**, 185–211.
- H. Wu, J. Yuan, Y. Bai, G. Pan, H. Wang and X. Shu, *J. Photochem. Photobiol., B*, 2012, **107**, 65–72.
- (a) P. M. May and D. R. Williams, in *Metal Ions in Biological Systems*, (Eds: H. Sigel), Marcel Dekker: New York, 1981, **12**; (b) T. Miura, A. Hori-i, H. Mototani and H. Takeuchi, *Biochemistry*, 1999, **38**, 11560–11569.
- S. Anbu, S. Shanmugaraju and M. Kandaswamy, *RSC Adv.*, 2012, **2**, 5349–5357.
- (a) D. Kong, J. Reibenspies, J. Mao, A. Clearfield and A. E. Martell, *Inorg. Chim. Acta*, 2003, **342**, 158–170; (b) S. Budagumpi, N. V. Kulkarni, G. S. Kurdekar, M. P. Sathisha and V. K. Revankar, *Eur. J. Med. Chem.*, 2010, **45**, 455–462.
- E. Meggers, *Curr. Opin. Chem. Biol.*, 2007, **11**, 287–292.
- (a) S. Anbu, R. Ravishankaran, A. A. Karande and M. Kandaswamy, *Dalton Trans.*, 2012, **41**, 12970–12983; (b) S. Tabassum, S. Amir, F. Arjmand, C. Pettinari, F. Marchetti, N. Masciocchi, G. Lupidi and R. Pettinari, *Eur. J. Med. Chem.*, 2013, **60**, 216–232.
- J. Ravichandran, P. Gurumoorthy, C. Karthick and A. K. Rahiman, *J. Mol. Struct.*, 2014, **1062**, 147–157.
- N. B. Colthrup, L. H. Daly and S. E. Wiberley, in *Introduction to Infrared and Raman Spectroscopy*, III Ed., Academic Press, San Diego, CA, 1990, 1–73.
- E. W. Ainscough, A. M. Brodie, J. D. Ranford and J. M. Waters, *J. Chem. Soc., Dalton Trans.*, 1997, 1251–1255.
- A. E. Underhill and D. E. Billing, *Nature*, 1966, **210**, 834–835.
- M. Chauhan, K. Banerjee and F. Arjmand, *Inorg. Chem.*, 2007, **46**, 3072–3082.
- Z. H. Chohan, H. A. Shad, L. Toupet, T. B. Hadda and M. Akkurt, *J. Chem. Crystallogr.*, 2011, **41**, 159–162.
- Y. -C. Liu, X. -Y. Song, Z. -F. Chen, Y. -Q. Gu, Y. Peng and H. Liang, *Inorg. Chim. Acta*, 2012, **382**, 52–58.
- G. R. Desiraju and T. Steiner, in *The Weak Hydrogen Bond in Structural Chemistry and Biology*, Oxford University Press, New York, 1999.
- A. W. Addison, T. N. Rao, J. Reedijk, J. van Rijn and G. C. Verschoor, *J. Chem. Soc., Dalton Trans.*, 1984, 1349–1356.
- M. B. Bushuev, Y. V. Gatilov, E. B. Nikolaenkova, V. G. Vasiliev and V. P. Krivopalov, *Inorg. Chim. Acta*, 2013, **395**, 95–103.
- W. J. Geary, *Coord. Chem. Rev.*, 1971, **7**, 81–122.
- P. A. Connick and K. A. Macor, *Inorg. Chem.*, 1991, **30**, 4654–4663.
- A. Benzekri, P. Dubourdeaux, J. M. Latour, P. Rey and J. Laugier, *J. Chem. Soc., Dalton Trans.*, 1991, 3359–3365.
- T. Atalay and E. Özkan, *Thermochim. Acta*, 1994, **237**, 369–374.
- M. J. Hossain, M. Yamasaki, M. Mikuriya, A. Kuribayashi and H. Sakiyama, *Inorg. Chem.*, 2002, **41**, 4058–4062.
- B. Bleaney and K. D. Bowers, *Proc. R. Soc. London A*, 1952, **214**, 451–465.
- W. Kaim and J. Rall, *Angew. Chem. Int. Ed. Engl.*, 1996, **35**, 43–60.
- A. P. Neves, K. C. B. Maia, M. D. Vargas, L. C. Visentin, A. Casellato, M. A. Novak and A. S. Mangrich, *Polyhedron*, 2010, **29**, 2884–2891.
- W. E. Marsh, K. C. Patel, W. E. Hatfield and D. J. Hodgson, *Inorg. Chem.*, 1983, **22**, 511–515.
- R. Cortés, L. Lezama, J. I. R. de Larramendi, G. Madariaga, J. L. Mesa, F. J. Zufiga and T. Rojo, *Inorg. Chem.*, 1995, **34**, 778–786.
- O. F. Ikotun, E. M. Higbee, W. Ouellette, F. Lloret, M. Julve and R. P. Doyle, *Eur. J. Inorg. Chem.*, 2008, 5281–5286.
- (a) C. S. Rivas, J. C. Espin and H. Wichers, *Phytochem. Anal.*, 2000, **11**, 330–338; (b) K. Tsai, T. G. Hsu, H. Cheng, T. Y. Liu, C. F. Hsu and C. W. Kong, *Free Radical. Biol. Med.*, 2001, **31**, 1465–1472.
- S. Ramakrishnan, V. Rajendiran, M. Palaniandavar, V. S. Periasamy, B. S. Srinag, H. Krishnamurthy and M. A. Akbarsha, *Inorg. Chem.*, 2009, **48**, 1309–1322.
- D. S. Raja, N. S. P. Bhuvanesh and K. Natarajan, *Eur. J. Med. Chem.*, 2011, **46**, 4584–4594.

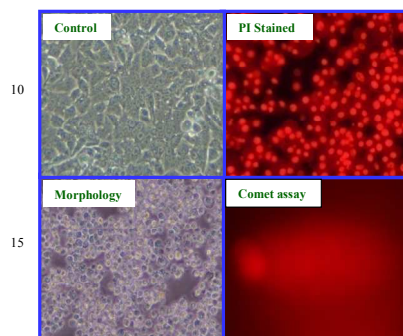
- 37 (a) S. A. Bejune, A. H. Shelton and D. R. McMillin, *Inorg. Chem.*, 2003, **42**, 8465–8475; (b) G. Dougherty and W. J. Pigram, *Crit. Rev. Biochem.*, 1982, **12**, 103–132.
- 38 M. T. Carter, M. Rodriguez and A. J. Bard, *J. Am. Chem. Soc.*, 1989, **111**, 8901–8911.
- 39 P. Zhao, L. C. Xu, J. W. Huang, K. C. Zheng, J. Liu, H. C. Yu and L. N. Ji, *Biophys. Chem.*, 2008, **134**, 72–83.
- 40 M. Cory, D. D. Mckee, J. Kagan, D. W. Henry and J. A. Miller, *J. Am. Chem. Soc.*, 1985, **107**, 2528–2536.
- 41 S. Satyanarayana, J. C. Dabrowiak and J. B. Chaires, *Biochemistry*, 1992, **31**, 9319–9324.
- 42 L. Jin and P. Yang, *J. Inorg. Biochem.*, 1997, **68**, 79–83.
- 43 E. J. Gabbay, R. E. Scofield and C. S. Baxter, *J. Am. Chem. Soc.*, 1973, **95**, 7850–7857.
- 44 H. -L. Chen, H. -Q. Liu, B. -C. Tzeng, Y. -S. You, S. -M. Peng, M. Yang and C. -M. Che, *Inorg. Chem.*, 2002, **41**, 3161–3171.
- 45 M. T. Carter and A. J. Bard, *J. Am. Chem. Soc.*, 1987, **109**, 7528–7530.
- 46 C. Tolia, A. N. Papadopoulos, C. P. Raptopoulou, V. Psycharis, C. Garino, L. Salassa and G. Psomas, *J. Inorg. Biochem.*, 2013, **123**, 53–65.
- 47 P. A. N. Reddy, M. Nethaji and A. R. Chakravarty, *Eur. J. Inorg. Chem.*, 2004, **7**, 1440–1446.
- 48 D. Desbouis, I. P. Troitsky, M. J. Belousoff, L. Spiccia and B. Graham, *Coord. Chem. Rev.*, 2012, **256**, 897–937.
- 49 A. Sreedhara and J. A. Cowan, *J. Biol. Inorg. Chem.*, 2001, **6**, 337–347.
- 50 N. A. Rey, A. Neves, P. P. Silva, F. C. S. Paula, J. N. Silveira, F. V. Botelho, L. Q. Vieira, C. T. Pich, H. Terenzi and E. C. P. -Maia, *J. Inorg. Biochem.*, 2009, **103**, 1323–1330.
- 51 B. K. Keppler and B. K. Holler, in *Metal complexes in Cancer Chemotherapy*, Wiley-VCH, Weinheim, 1993, 37.
- 52 N. Milhazes, T. C. -Oliveira, P. Martins, J. Garrido, C. Oliveira, A. C. Rego and F. Borges, *Chem. Res. Toxicol.*, 2006, **19**, 1294–1304.
- 53 I. M. Ghobrial, T. E. Witzig and A. A. Adjei, *Cancer J. Clin.*, 2005, **55**, 178–194.
- 54 P. Moller, L. E. Knudsen, S. Loft and H. Wallin, in *Cancer Epidemiol. Biomarkers Prevent.*, 2000, **9**, 1005–1015.
- 55 C. Alapetite, *Int. J. Radiat. Biol.*, 1996, **69**, 359–369.
- 56 (a) R. Prabhakaran, P. Kalaivani, P. Poornima, F. Dallemer, G. Paramaguru, V. Vijaya Padma, R. Renganathan, R. Huang and K. Natarajan, *Dalton Trans.*, 2012, **41**, 9323–9336; (b) K. Dhahagani, S. Mathan Kumar, G. Chakkaravarthi, K. Anitha, J. Rajesh, A. Ramu and G. Rajagopal, *Spectrochim. Acta Part A*, 2014, **117**, 87–94.
- 57 Bruker-Nonius, in *APEX-II and SAINT-plus* (Version 7.06a), Bruker AXS Inc., Madison, Wisconsin, USA, 2004.
- 58 A. Altomare, G. Cascarano, C. Giacovazzo and A. Guagliardi, *J. Appl. Crystallogr.*, 1993, **26**, 343–350.
- 59 M. Sheldrick, *Acta Crystallogr., Sec. A*, 2008, **64**, 112–122.
- 60 L. J. Farrugia, *J. Appl. Crystallogr.*, 1997, **30**, 565.
- 61 C. F. Macrae, P. R. Edgington, P. McCabe, E. Pidcock, G. P. Shields, R. Taylor, M. Towler and J. van de Streek, *J. Appl. Crystallogr.*, 2006, **39**, 453–457.
- 62 (a) M. Cuendet, K. Hostettmann and O. Potterat, *Helv. Chim. Acta*, 1997, **80**, 1144–1152; (b) M. Burits and F. Bucar, *Phytother. Res.*, 2000, **14**, 323–328.
- 63 J. Marmur, *J. Mol. Biol.*, 1961, **3**, 208–218.
- 64 R. Reichmann, S. A. Rice, C. A. Thomas and P. Doty, *J. Am. Chem. Soc.*, 1954, **76**, 3047–3053.
- 65 G. Cohen and H. Eisenberg, *Biopolymers*, 1969, **8**, 45–55.
- 66 S. Mahadevan and M. Palaniandavar, *Bioconjugate Chem.*, 1996, **7**, 138–143.
- 67 T. Mosmann, *J. Immunol. Methods*, 1983, **65**, 55–63.
- 68 G. Chandrasekher and D. Sailaja, *Invest. Ophthalmol. Vis. Sci.*, 2004, **45**, 3577–3588.
- 69 O. Östling and K. J. Johanson, *Biochem. Biophys. Res. Commun.*, 1984, **123**, 291–298.
- 70 (a) V. J. McKelvey-Martin, M. H. Green, P. Schmezer, B. L. Pool-Zobel, M. P. De Meo and A. Collins, *Mutat. Res.*, 1993, **288**, 47–63; (b) A. R. Collins, *Mol. Biotechnol.*, 2004, **26**, 249–261.
- 71 N. P. Singh, M. T. MacCoy, R. R. Tice and E. L. Schneider, *Exp. Cell Res.*, 1988, **175**, 184–191.

# Magneto-structural correlation, antioxidant, DNA interaction and growth inhibition activities of new chloro-bridged phenolate complexes

Perumal Gurumoorthy,<sup>a</sup> Dharmasivam Mahendiran,<sup>a</sup> Durai Prabhu,<sup>b</sup> Chinnasamy Arulvasu<sup>b</sup> and Aziz Kalilur Rahiman,<sup>\*a</sup>

5

## Table of Contents



10

15

## 20 Highlights

The consistent stability constants as well as antioxidant, DNA interaction and cytotoxicity efficacy of chloro-bridged complexes have been established.